The Late-Stage Steps of *Burkholderia cenocepacia* Protein *O*-Linked Glycan Biosynthesis Are Conditionally Essential.

Leila Jebeli[1], Taylor A. McDaniels[1], Duncan T. T. Ho[1], Hamza Tahir[1], Nicholas L. Kai-Ming[1], Molli Mcgaw[1], Kristian I. Karlic[1], Jessica M. Lewis[2] and Nichollas E. Scott[1]

[1]Department of Microbiology and Immunology, University of Melbourne at the Peter Doherty Institute for Infection and Immunity, Melbourne 3000, Australia

Current addresses:

[2]School of Life Sciences, University of Warwick, Coventry, CV4 7AL, UK.

[#]To whom correspondence and requests for materials should be addressed N.E.S (Nichollas.scott@unimelb.edu.au)

Key words: Glycosylation, *Burkholderia cenocepacia*, *Burkholderia*, Post-translational modifications, Proteomics, Glycoproteomics

Abstract:

Periplasmic *O*-linked protein glycosylation is a highly conserved process observed across the *Burkholderia* genus. Within Burkholderia, protein glycosylation requires the five gene cluster known as the *O*-glycosylation cluster (OGC, *ogcXABEI*) which facilitates the construction of the *O*-linked trisaccharide attached to periplasmic proteins. Previous studies have reported conflicting results regarding the essentiality of *ogcA*, predicted to be responsible for the addition of the final carbohydrate of the *O*-linked trisaccharide and *ogcX,* the putative *O*-linked glycan flippase. Within this work, we aimed to dissect the impact of the loss of *ogcA* and *ogcX* on *Burkholderia cenocepacia* viability. We demonstrate that the loss of either *ogcA* or *ogcX* are detrimental if glycosylation is initiated leading to marked phenotypic effects. Proteomic analysis supports that the loss of *ogcA*/*ogcX* both blocks glycosylation and drives pleotropic effects in the membrane proteome, resulting in the loss of membrane integrity. Consistent with this, strains lacking *ogcA* and *ogcX* exhibit increased sensitivity to membrane stressors including antibiotics and demonstrate marked changes in membrane permeability. These effects are consistent with fouling of the undecaprenyl pool due to dead-end *O*-linked glycan intermediates, and consistent with this, we show that modulation of the undecaprenyl pool through the overexpression of undecaprenyl pyrophosphate synthase (UppS) or the OGC flippase (OgcX) restores viability while expression of early-stage OGC biosynthesis genes (*ogcI* and *ogcB*) reduce *B. cenocepacia* viability. These findings demonstrate disrupting *O*-linked glycan biosynthesis or transport appears to dramatically impact *B. cenocepacia* viability, supporting the assignment of *ogcA* and *ogcX* as conditionally essential.

Importance:

Protein glycosylation, a conserved process in *Burkholderia* species, utilizes glycans generated by the *O*-glycosylation cluster (OGC), which is composed of five genes (*ogcX, ogcA*, *ogcB*, *ogcE*, and *ogcI*). In this study, we demonstrate that the loss of *ogcA* or *ogcX* significantly affects the physiology of *Burkholderia cenocepacia*. Using complementary genetic approaches and proteomic techniques, we show that the loss of *ogcA* or *ogcX* blocks glycosylation, alters the cell membrane, and sensitizes cells to stressors such as antibiotics. This increased sensitivity to membrane stress is consistent with the accumulation of dead-end *O*-linked glycan intermediates, which sequester the limited and essential undecaprenyl pool within *B. cenocepacia*. These findings highlight that *ogcA* and *ogcX* are conditionally essential for *B. cenocepacia* survival and provides mechanistic insight into how protein glycosylation fidelity—the use of specific glycans for protein glycosylation—is controlled in *Burkholderia* species.

55 **Introduction:**

56 Across bacterial species many surface polysaccharides are synthesized utilising the essential
57 polyisoprenoid lipid undecaprenyl phosphate (Und-P) [1,2]. Functioning as a chemical carrier,
58 Und-P provides an assembly point for the stepwise construction of diverse lipid-linked
59 oligosaccharide units at the inner face of the cytoplasmic membrane within Gram-negative
60 and Gram-positive species [1,2]. By providing a tethering point to enable glycan elongation,
61 Und.P allows the construction of a range of glycans, which upon translocation across the
62 cytoplasmic membrane can be integrated into glycoconjugates including peptidoglycan, cell
63 wall teichoic acids, O-antigens, capsules, and exopolysaccharides [3,4]. While Und-P and its
64 phosphorylated form undecaprenyl pyrophosphate (Und-PP) are important for the
65 construction of surface carbohydrates, these molecules account for less than 1% of the total
66 lipid pool [5], resulting in competition for available Und-P and the need for rapid flux of
67 oligosaccharide units through the Und-P/Und-PP cycle [6,7]. Under normal physiological
68 conditions, *de novo* synthesis and recycling of Und-P/Und-PP are able to meet physiological
69 demands [6,7], yet it is increasingly recognised that genetic manipulations that result in Und-
70 PP-glycan intermediates that sequester the Und-P/Und-PP pool can dramatically impact
71 cellular viability, morphology and growth [6-11]. Understanding Und-PP-glycan intermediates
72 with the capacity to foul the Und-P/Und-PP pool has the potential to not only aid
73 antimicrobial development [12,13] but also explain the mechanisms underpinning the
74 homogeneity observed within the glycan structures of glycoconjugates [14-16].

75 Ensuring only glycans possessing specific structural configurations, herein referred to as
76 glycan fidelity, are translocated across the cytoplasmic membrane ensures homogeneity
77 within oligosaccharide units constructed utilising the Und-P/Und-PP pool [3,4]. For many
78 glycoconjugates generated using Und-PP linked oligosaccharides, the addition of specific
79 glycan components is a pre-requisite for effective translocation across the cytoplasmic
80 membrane by the actions of dedicated translocases known as flippases [17-19]. Of the known
81 flippases the Wzx enzymes represent a highly diverse family of enzymes [19,20] responsible for
82 the translocation of a range of carbohydrates including O-antigens [21], capsules [22,23],
83 exopolysaccharides [24], and the enterobacterial common antigen (ECA) [10]. While Wzx
84 flippases were initially thought to possess limited capacity for the recognition of glycan
85 structures [25,26], it has become clear multiple features of their cognate glycans, such as

specific branching or terminal sugars in addition to the initiating sugar influence translocation efficiency when Wzx enzymes are expressed under native-like conditions [3,15,27,28]. This specificity results in discrete Wzx flippases being observed genetically linked to their cognate glycan clusters [15,22,23,27] with Wzx enzymes suggested to function as quality control mechanisms [16], ensuring only "complete" glycans are effectively translocated across the cytoplasmic membrane. The specificity for complete glycans by Wzx flippases in concert with the extension of glycans beyond key points commit Und-PP-linked oligosaccharides to the generation of specific glycans [11,25,29-32]. In cases where Und-PP-linked intermediates are unable to be completed this drives detrimental phenotypes due to the sequestration of the Und-P/Und-PP pool including growth defects, enhanced sensitivity to membrane stresses and alterations in cellular morphology [6,7,11]. Importantly the profound effects of Und-P/Und-PP sequestration is known to rapidly lead to the emergence of suppressor mutations, which complicates the analysis of Und-P/Und-PP glycan biosynthesis pathways by obfuscating the role of specific glycan biosynthesis genes [9,33,34]. While these potential confounding effects are now well appreciated for the O-antigens [6,11], capsule [35] and ECA [7], this phenomenon has not been explored within glycans used for other glycoconjugates such as protein glycosylation.

Protein glycosylation is widespread across bacterial species [36,37] including members of the *Campylobacter* [38,39], *Neisseria* [40-44], and *Burkholderia* [45-47] genera. To date, several Und-P/Und-PP dependent glycosylation systems have been described in Gram-negative species, which utilise the Und-P lipid pool to enable periplasmic glycosylation leading to glycosylation of tens to hundreds of proteins [37,48-50]. While similarities within the biosynthetic clusters used for protein glycosylation systems and lipooligosaccharide biosynthetic clusters have been previously highlighted [36,37], a notable difference within well-characterised glycosylation systems is the use of ABC transporter-based flippases [36,37] as opposed to Wzx flippases. ABC transporter-based flippases, such as PglK (also known as WlaB[51]) within *Campylobacter* sp. [52,53] and PglF within *Neisseria* sp. [54-56] are dispensable for glycosylation [53,56] as well as possess relaxed glycan specificities as demonstrated using heterogenous expression studies for PglK [53] and the observation of glycan microheterogeneity within *Neisseria* [57,58]. The tolerance of these glycosylation pathways to both glycan alterations, as well as the loss of their flippases, is in stark contrast to the strict

117 specificity and essentiality seen within other Und-P/Und-PP dependent systems, yet not all
118 Und-P/Und-PP dependent protein glycosylation systems possess ABC transporter flippases.

119 Within *Burkholderia* species, periplasmic glycosylation is highly conserved [45-47], leading to
120 nearly exclusive modification of serine residues [45] with a trisaccharide corresponding to β-
121 Gal-(1,3)–α-GalNAc-(1,3)–β-GalNAc [47]. *Burkholderia O*-linked glycan assembly is mediated by
122 a single gene cluster known as the O-linked Glycosylation Cluster (*OGC*) consisting of five
123 genes (*ogcX*, *A*, *B*, *E* and *I* corresponding to BCAL3114 to BCAL3118 within *Burkholderia*
124 *cenocepacia* respectively) [47]. Our current model of glycan assembly (**Figure 1A**) supports
125 OgcE (BCAL3117) as a UDP-Glc / UDP-GlcNAc epimerase, OgcI (BCAL3118) as the initiating
126 glycotransferase for the *O*-linked glycan, OgcB (BCAL3116) and OgcA (BCAL3115) work as
127 extending glycosyltransferases responsible for the addition of the second GalNAc and final
128 Gal residues respectively, and the putative Wzx flippase OgcX (BCAL3114), responsible for
129 the translocation of the glycan across the cytoplasmic membrane [47] where it can then be
130 transferred to glycoproteins by the oligosaccharyltransferase PglL (BCAL0960) [47,59]. Previous
131 studies have provided experimental evidence for the function of OgcB, OgcE and OgcI [47] yet
132 contradictory results have been obtained for the enzymes OgcA and OgcX. While it has been
133 noted that despite multiple attempts an *ogcA* knockout has been unable to be generated [47],
134 the loss of *ogcX* has been previously reported to be tolerated within *B. cenocepacia* [47].
135 Similarly, saturation transposon studies from several *Burkholderia* species [60-62] have
136 revealed variability in the ability to disrupt *ogcA* and *ogcX,* with some studies concluding
137 these enzymes are essential [62] while others suggest that at least for *ogcA* disruptions within
138 this gene may be tolerated [61]. These observations support that unlike the glycosylation
139 systems of the *Campylobacter* and *Neisseria* genera, disruptions in glycan biosynthesis steps
140 may not be tolerated within *Burkholderia.* These contradictory results support further
141 assessments are required to dissect the impact of loss of *ogcA* and *ogcX* on viability and
142 protein glycosylation.

143 Within this work, we sought to assess the requirement of *ogcA* and *ogcX* for protein
144 glycosylation and the impact of the loss of these *ogc* components on *B. cenocepacia.*
145 Utilising complementary genetic approaches, including *ogc* complementation within strains
146 lacking the *ogc* cluster [47,63] as well as glycosylation inducible strains containing the initiating
147 transferase, *ogcI,* under rhamnose control [64], we assess the proteomic and physiological

impacts of the loss of *ogcA* and *ogcX.* We demonstrate that in the absence of glycosylation initiation, *ogcA* and *ogcX* are dispensable, yet upon glycosylation initiation, loss of these genes leads to growth defects, widespread proteomic impacts, changes in the membrane integrity and the absence of observable glycosylation. While these changes can be complemented and compensated by the modulation of enzymes associated with *de novo* synthesis of Und-P as well as the overexpression of the flippase OgcX, we observe that the modulation of early steps in the *O*-linked glycan biosynthesis pathways can also drive changes in viability. This data supports that the construction of the *O*-linked glycan in *B. cenocepacia* is finely tuned with *ogcA* and *ogcX* conditionally detrimental if glycosylation is initiated.

159 **Methods:**

160 **Bacterial strains and growth conditions:** Bacterial strains used in this study are listed in
161 **Supplementary Table 1**. Strains were cultured in Lysogeny Broth (LB) or on LB agar (1.5–2%
162 w/v), prepared in accordance with the manufacturer's instructions containing 0.5% NaCl
163 (BD™, New Jersey, USA). Liquid cultures were incubated overnight at 37°C with shaking,
164 while agar plates were incubated at 37°C overnight for *Escherichia coli* and 24–72 hours for
165 *B. cenocepacia*. When required, LB was supplemented with 200 µg/mL diaminopimelic acid
166 (DAP; Sigma) to support growth of *E. coli* RHO3 [65]. Antibiotics were added to cultures to
167 select or maintain plasmids/ transconjugants at a final concentration of 50 µg/mL
168 trimethoprim for *E. coli* and 100 µg/mL for *B. cenocepacia*, 20 µg/mL tetracycline for *E. coli*
169 and 150 µg/mL for *B. cenocepacia* and 50 µg/mL kanamycin for *E. coli*. To counter-select
170 helper and donor *E. coli* strains during triparental and quadparental mating, ampicillin at
171 100 µg/mL and polymyxin B at 25 µg/mL were added [66]. Culturing of strains containing the
172 temperature-sensitive plasmid pFlptet (see **Supplementary Table 2**) was undertaken at 30°C
173 with cultures shifted to 37°C to enable plasmid curing [67]. Curing of pDAI-SceI-SacB was
174 achieved by sucrose counterselection as previously described with 5% sucrose in LB lacking
175 NaCl [66]. Induction of *B. cenocepacia* strains was performed by either adding 20% filter-
176 sterilised L-rhamnose monohydrate (Sigma) or 1 mM 4-Isopropylbenzoic acid (cumate,
177 Sigma) to LB broth or LB agar at a concentration of 0.05%-1% for rhamnose and 100 µM for
178 cumate. For non-induced controls, an equivalent volume of solvent (sterile water for
179 rhamnose and ethanol for cumate) was added to the culture media.

180

181 **Recombinant DNA methods:** Oligonucleotides used in this study are listed in
182 **Supplementary Table 3**, with all PCR amplifications for cloning carried out using Q5 DNA
183 polymerase (New England Biolabs) with the addition of 2% DMSO for the amplification of
184 *B. cenocepacia* DNA, due to its high GC content. Genomic DNA isolations were performed
185 using an EZ-10 Spin Column Bacterial Genomic DNA Mini-Preps Kit (Bio Basic), while PCR
186 clean up and restriction digest purifications were performed with a Zymoclean Gel DNA
187 Recovery Kit (ZymoResearch). pGPI-SceI [68] mutagenesis plasmids were constructed using
188 Gibson assembly [69] with DNA fragments flanking genes of interest amplified by Q5-based

189 PCR. *Sma*I-linearized pGPI-SceI and Q5-amplified fragments were assembled using the
190 NEBuilder® HiFi DNA master mix according to the manufacturer's instructions (New England
191 Biolabs). pSCrhaB2 [64] and pMLBAD [70] based expression vectors containing genes of interest
192 were generated using Gibson Assembly or restriction endonuclease-based cloning. For
193 Gibson Assembly, PCR-amplified fragments were introduced into *Nde*I/*Xba*I-linearized
194 pSCrhaB2 or PCR-derived pMLBAD vector backbones using the NEBuilder® HiFi DNA master
195 mix. For restriction endonuclease-based cloning, PCR-amplified fragments were digested
196 with *Nde*I/*Xba*I and then ligated into *Nde*I/*Xba*I-linearized pSCrhaB2 overnight at 16°C using
197 T4 Ligase (New England Biolabs). Mutagenesis of pSCrhaB2-ogc to remove *ogc*A, *ogc*B, *ogc*I
198 and *ogc*X was achieved by assembling PCR-amplified fragments into *Nde*I/*Hind*III-linearized
199 pSCrhaB2 using the NEBuilder® HiFi DNA master mix.

200 Prior to Gibson Assembly and restriction cloning all DNA fragments were assessed for
201 correctness based on size using agarose gel electrophoresis. Ligated/assembled plasmid
202 mixtures were introduced into chemically competent *E. coli* PIR2 cells via heat shock
203 transformation [71], plated on selective media and screened using colony PCR with GoTaq®
204 Green Master Mix (Promega). All plasmids used in this study have been confirmed by either
205 Sanger sequencing using the Australian Genome Research Facility (Melbourne, Australia) or
206 nanopore plasmid sequencing using Plasmidsaurus (SNPsaurus LLC, Eugene, OR). Donor
207 plasmids for biparental and quadparental mating were further isolated and introduced into
208 *E. coli* RHO3 [65] via electroporation [71] to improve conjugation efficiency into
209 *B. cenocepacia*. A complete list of the plasmids used in this study, along with a summary of
210 their construction, is provided in **Supplementary Table 2**.

211

212 **Conjugation of plasmids into *B. cenocepacia*:** Plasmids were introduced into *B. cenocepacia*
213 K56-2 via one of three approaches: I) biparental mating using the conjugative
214 diaminopimelic acid auxotroph *E. coli* RHO3 [65] for the introduction of pFLPtet or pDAI-SceI-
215 SacB; II) triparental mating [66] using *E. coli* PIR2 containing pRK2013 (helper plasmid) [72] and
216 *E. coli* PIR2 carrying pGPI-SceI-derived vectors or pSCrhaB2/pMLBAD expression vectors
217 (donor plasmid); or III) quadparental mating using *E. coli* PIR2 containing pRK2013 [72], *E. coli*
218 PIR2 containing pTNS3 (Tn7 transposase plasmid) [73] and *E. coli* RHO3 carrying pUC18T-mini-

219 Tn7T-Tp-rha-ogcI (donor plasmid) for the chromosomal integration of miniTn7-rha-ogcI.
220 Conjugations were allowed to proceed for 24 hours, then successful transconjugants were
221 selected with trimethoprim, and the introduction of plasmids of interest confirmed using
222 PCR-based screening. For the generation of unmarked, non-polar deletions using pGPI-SceI
223 and the removal of the trimethoprim resistance marker within the integrated miniTn7,
224 additional rounds of conjugation were undertaken to introduce pDAI-SceI-SacB [68,74] or
225 pFLPtet[67] respectively using tetracycline based selection. pGPI-SceI/pDAI-SceI-SacB-based
226 mutagenesis as well as FLP-based removal of the trimethoprim resistance marker within Tn7
227 were confirmed using screening oligonucleotides (**Supplementary Table 3**) by colony PCR
228 using GoTaq® Green Master Mix. Numeration of transconjugants derived from the
229 introduction of pSCrhaB2-*ogc* and its derivatives into *B. cenocepacia* wildtype (WT) or
230 *B. cenocepacia* Δ*ogc* were assessed across three independent conjugations.

231

232 **Spot plate assays:** Colony size morphology and membrane stress tolerance assessments
233 were performed as previously described [75-77] using spot plate assays. For spot plate assays,
234 strains of interest were grown overnight in LB broth without induction, normalised to an
235 OD_{600} of 1.0 and then serially diluted from 10^{-1} to 10^{-6}. 10 µL of diluted cultures were
236 manually spotted onto LB plates with and without inducers (1% Rhamnose /100 µM
237 cumate). 0.01% SDS or 2% NaCl were added to plates to assess membrane integrity and the
238 impact of osmotic stress on viability with and without inducers. For assays of *B. cenocepacia*
239 strains containing pSCrhaB2- or pMLBAD-based expression vectors, trimethoprim was
240 added to plates to ensure the maintenance of plasmids. For antimicrobial resistance, spot
241 assays concentrations corresponding to at or below the broth dilution defined MIC assays
242 (**Supplementary Figure 10**) were used for trimethoprim (8 µg/mL), tetracycline (16 µg/mL),
243 chlorhexidine (4 µg/mL), ceftazidime (4 µg/mL), and rifampicin (32 µg/mL) on cation-
244 adjusted Mueller–Hinton agar. Spots were allowed to dry, and plates were incubated for 48
245 hours at 37°C before being imaged. All spot assays were assessed using at least three
246 independent replicates. Colony area measurements were undertaken using Fiji [78], assessing
247 the size of 20 colonies per spot assay with three independent assays conducted with t-tests
248 used to determine significant changes in colony size as well as viable counts between
249 induced and non-induced conditions.

250

251 **Microtiter plate-based viability and growth kinetics assays.** To assess viability and growth
252 kinetics, Microtiter 96-well-based growth assays were undertaken as previously described
253 [63]. Bacterial strains were grown overnight in LB, normalised to an OD_{600} of 1.0 and diluted 1
254 in 100 with LB supplemented with or without combinations of inducers and/or membrane
255 stressors (0.01% SDS or 2% NaCl). 200 µL of diluted cultures were added to 96-well flat-
256 bottom plates and incubated at 37°C with shaking at 200 rpm in a CLARIOstar plate reader
257 (BMG LABTECH, Inc.), measuring the optical density at 600 nm every 10 minutes over 24
258 hours. Growth assays were assessed in at least technical triplicate across three independent
259 biological replicates.

260

261 **Fluorescence Detection of the permeability of inner and outer membranes:** Permeability
262 of the inner membrane was assessed using Hoechst 33342 (Abcam) as previously described
263 [79-81]. Briefly, bacterial strains were grown overnight in LB (with and without 1% Rhamnose),
264 normalised to an OD_{600} of 2.0, washed three times with PBS and dispensed at 100 µL
265 aliquots into 96-well black clear-bottomed plates. 100 µL of PBS and heat-killed bacteria
266 were added to the plates as controls. 100 µL of 2.5 µM Hoechst 33342 in PBS was added to
267 wells to generate bacterial suspensions with an OD_{600} of 1.0 and a final concentration of
268 1.25 µM Hoechst 33342. Fluorescence was measured in a CLARIOstar plate reader using an
269 excitation of 361nm and emission detection at 486nm. The fluorescence intensity was first
270 normalised by assigning the value of 100 to the heat-killed and 0 to the non-induced
271 parental strain. To assess outer membrane permeability, 1-*N*-phenylnaphthylamine (NPN,
272 Thermo Fisher Scientific) as previously described [82-84]. Cultures were normalised as above,
273 washed three times with 5 mM HEPES, pH 7.4, 10 mM sodium azide and dispensed at 100
274 µL aliquots into 96-well black clear-bottomed plates. 100 µL of 5 mM HEPES, pH 7.4, 10 mM
275 sodium azide was added to the plates as a blank. 100 µL of 20 µM NPN in 5 mM HEPES, pH
276 7.4, 10 mM sodium azide was added to wells to generate bacterial suspensions with an
277 OD_{600} of 1.0 and a final concentration of 100 µM NPN. Fluorescence was measured in a
278 CLARIOstar plate reader using an excitation of 350nm and emission detection at 420nm.
279 Hoechst 33342 and NPN assays were assessed in technical triplicate across five independent

280 biological replicates comparing changes in fluorescence intensity to the non-induced
281 parental strain. To assess viability and ensure comparable cell numbers, the OD-adjusted
282 bacterial suspensions were serially diluted and plated on LB and viable cells numerated
283 (**Supplementary Figure 11**). The fluorescence intensity from both assays was normalised
284 against the determined cell number.

285

286 **Preparation of proteomic samples:** *B. cenocepacia* cultures for proteomic analysis were
287 grown overnight with or without induction with rhamnose and cumate as outlined above
288 with shaking at 180 rpm. Overnight cultures were normalised to an OD_{600} of 1.0 and then
289 collected by centrifugation at 10,000 x *g* at 4˚C for 10 minutes, washed 3 times with ice-cold
290 PBS and then snap frozen at -80˚C until processing. Frozen whole cell samples were
291 prepared for analysis using sodium deoxycholate (SDC) based lysis and the in-StageTip
292 preparation approach as previously described [85]. OgcX complementation assays were
293 undertaken using SDS-based lysis and S-trap sample preparation to improve the detection of
294 OgcX. For in-StageTip preparation, cells were resuspended in 4% SDC, 100 mM Tris pH 8.0
295 and boiled at 95˚C with shaking (2000 rpm) for 10 minutes to solubilise the proteome.
296 Samples were allowed to cool for 10 minutes and then boiled for a further 10 minutes (95°C,
297 2000 rpm) before the protein concentrations were determined by bicinchoninic acid assays
298 (Thermo Fisher Scientific). Samples were reduced/alkylated with the addition of Tris-2-
299 carboxyethyl phosphine and chloroacetamide (final concentration 10 mM and 40 mM,
300 respectively), and samples were incubated in the dark for 0.5-1 hour at 45˚C. Following
301 reduction/alkylation, samples were digested overnight with Trypsin (1/50 w/w Solu-trypsin,
302 Sigma) at 37˚C with shaking at 1000rpm. Digests were then quenched with the addition of
303 1.25 volumes of isopropanol before being cleaned up using SDB-RPS (Sigma) StageTips.

304 For S-trap-based preparation, cells were resuspended in 4% sodium dodecyl sulphate (SDS),
305 100 mM Tris pH 8.0, and boiled at 95˚C with shaking (2000 rpm) for 10 minutes; the protein
306 concentrations were then determined by bicinchoninic acid assays, and samples were
307 reduced/alkylated as above. Samples were acidified to 1.2% phosphoric acid and diluted
308 with seven volumes of S-trap wash buffer (90% methanol, 100mM tetraethylammonium
309 bromide pH 7.1) before being loaded onto S-trap mini spin columns (Protifi) and washed 3

310 times with 400 µL of S-trap wash buffer. Samples were then digested with 2 µg of Trypsin (a
311 1:50 protease/protein ratio) in 100 mM tetraethylammonium bromide overnight at 37 °C
312 before being collected by centrifugation with washes of 100 mM tetraethylammonium
313 bromide, followed by 0.2% formic acid followed by 0.2% formic acid / 50% acetonitrile
314 before being dried by vacuum centrifugation at room temperature and stored at -20˚C.

315 SDB-RPS StageTip-based clean-up of digests was undertaken by adjusting or resuspending
316 samples in 50% isopropanol, 1% trifluoroacetic acid and then loading them on in-house
317 created SDB-RPS StageTips, which were prepared according to previously described
318 protocols [85-87]. Briefly, five frits of SDB-RPS were excised using a blunt 16-gauge Hamilton
319 needle and loaded into 200 µL tips. SDB-RPS StageTips were placed in a Spin96 tip holder [86]
320 to enable batch-based spinning of samples and tips conditioned with 100% acetonitrile,
321 followed by 30% methanol, 1% trifluoroacetic acid, followed by 90% isopropanol, 1%
322 trifluoroacetic acid with each wash spun through the column at 1000 x *g* for 3 minutes.
323 Acidified isopropanol/peptide mixtures were loaded onto the SDB-RPS columns and spun
324 through tips before being washed with 90% isopropanol, 1% trifluoroacetic acid, followed by
325 90% ethyl acetate, 1% trifluoroacetic acid, followed by 1% trifluoroacetic acid in Milli-Q
326 water. Peptide samples were eluted with 80% acetonitrile, 5% ammonium hydroxide and
327 dried by vacuum centrifugation at room temperature and stored at -20˚C.

328

329 **LC-MS analysis of DDA samples.** Cleaned-up peptide samples were re-suspended in Buffer
330 A* (2% acetonitrile, 0.1% trifluoroacetic acid in Milli-Q water) and separated using a two-
331 column chromatography set-up on a Dionex Ultimate 3000 UPLC composed of a PepMap100
332 C18 20 mm x 75 µm trap and a PepMap C18 500 mm x 75 µm analytical column (Thermo
333 Fisher Scientific) coupled to a Orbitrap Fusion™ Lumos™ Tribrid™ Mass Spectrometer
334 (Thermo Fisher Scientific) with datasets collected with and without the use of the FAIMS Pro
335 interface (Thermo Fisher Scientific). 145-minute gradients were run for each sample, with
336 samples loaded onto the trap column with 98% Buffer A (2% acetonitrile, 0.1% formic acid in
337 Milli-Q water) and 2% Buffer B (80% acetonitrile, 0.1% formic acid) with peptides separated
338 by altering the buffer composition from 2% Buffer B to 28% B over 126 minutes, then from
339 28% B to 40% B over 9 minutes, then from 40% B to 80% B over 3 minutes, the composition

340 was held at 80% B for 2 minutes, and then dropped to 2% B over 2 minutes and held at 2% B
341 for another 3 minutes. For datasets collected without the use of the FAIMS Pro interface,
342 the Lumos™ Mass Spectrometer was operated in a data-dependent mode, switching
343 between the collection of a single Orbitrap MS scan (450-2000 m/z, maximal injection time
344 of 50 ms, an Automatic Gain Control (AGC) of maximum of $4*10^5$ ions and a resolution of
345 60k) acquired every 3 seconds followed by Orbitrap MS/MS HCD scans of precursors (NCE
346 30%, maximal injection time of 80 ms, an AGC set to a maximum of $1.25*10^5$ ions and a
347 resolution of 30k). For datasets collected with the FAIMS Pro interface, a data-dependent
348 stepped FAIMS approach was utilised with three different FAIMS CVs -25, -45 and -65, as
349 previously described [88]. For each FAIMS CV a single Orbitrap MS scan (450-2000 m/z,
350 maximal injection time of 50 ms, an AGC of maximum of $4*10^5$ ions and a resolution of 60k)
351 was acquired every 1.2 seconds followed by Orbitrap MS/MS HCD scans of precursors (NCE
352 30%, maximal injection time of 80 ms, an AGC set to a maximum of $1.25*10^5$ ions and a
353 resolution of 30k). HCD scans containing HexNAc-associated oxonium ions (204.0867,
354 138.0545 and 366.1396 m/z) triggered two additional product-dependent MS/MS scans [89]
355 of potential glycopeptides; an Orbitrap EThcD scan (NCE 15%, maximal injection time of 150
356 ms, AGC set to a maximum of $2*10^5$ ions with a resolution of 30k using the extended mass
357 range setting to improve the detection of high mass glycopeptide fragment ions [90]) and a
358 stepped collision energy HCD scan (using NCE 35% with 5% Stepping, maximal injection time
359 of 150 ms, an AGC set to a maximum of $2*10^5$ ions and a resolution of 30k).

360

361 **LC-MS analysis of DIA samples:** Cleaned-up peptide samples were resuspended in Buffer A*
362 and separated using a two-column chromatography set-up on a Dionex Ultimate 3000 UPLC
363 composed of a PepMap100 C18 20 mm x 75 µm trap and a PepMap C18 500 mm x 75 µm
364 analytical column. Samples were concentrated onto the trap column at 5 µL/min for 5
365 minutes with 98% Buffer A and 2% Buffer B, then infused into an Orbitrap Fusion™ Lumos™
366 Tribrid™ Mass Spectrometer at 300 nL/minute via the analytical column. 125-minute
367 analytical runs were undertaken by altering the buffer composition from 3% Buffer B to 25%
368 B over 112 minutes, then from 25% B to 40% B over 4 minutes, then from 40% B to 80% B
369 over 1 minute. The composition was held at 80% B for 3 minutes and then dropped to 3% B
370 over 1 minute before being held at 3% B for another 4 minutes. Data was collected in a

Data-independent manner with a single MS1 event (120k resolution, AGC $1*10^6$, 350-1400 m/z) and 50 MS2 scans (NCE 30%, 30k resolution, AGC $1*10^6$, 200-2000 m/z and a maximal injection time of 55 ms) of a width of 13.7 m/z collected over the mass range of 360 to 1033.5 m/z.

DDA-based proteomic analysis: DDA datasets were analysed using MSFragger (versions 18.0, 19.0, 20.0 or 22.0) [91-93]. Samples were searched with a Tryptic specificity, allowing a maximum of two missed cleavage events and Carbamidomethyl set as a fixed modification of Cysteine while oxidation of Methionine allowed as a variable modification. For searches to identify canonical Bukrholderia glycosylation the *Burkholderia* glycans $HexHexNAc_2$ (elemental composition: $C_{22}O_{15}H_{36}N_2$, mass: 568.2115 Da) and Suc-$HexHexNAc_2$ (elemental composition: $C_{26}O_{18}H_{40}N_2$, mass: 668.2276 Da) were included as variable modifications at Serine in line with the strong preference for PglL glycosylation at Serine residues [45]. To allow the assessment of glycoforms within strains lacking *ogc* genes the *Burkholderia* glycans $HexHexNAc_2$, Suc-$HexHexNAc_2$, $HexNAc_2$ (elemental composition: $C_{16}O_{10}H_{26}N_2$, mass: 406.1488 Da) and HexNAc (elemental composition: $C_8O_5H_{13}N$, mass: 203.0794 Da) were included as variable modifications at Serine. For all glycopeptide searches the glycan fragment ions were defined as 204.0866, 186.0760 168.0655, 366.1395, 144.0656, 138.0550, 466.1555 and 407.1594. A maximum mass precursor tolerance of 20 ppm was allowed at both the MS1 and MS2 levels. Samples were searched against the *B. cenocepacia* reference proteome J2315 (Uniprot accession: UP000001035, 6,993 proteins, downloaded July 24th 2020) [94] supplemented with the proteins RhaS (HTH-type transcriptional activator RhaS, P09377), RhaR (HTH-type transcriptional activator RhaR, P09378), TmpR (Dihydrofolate reductase resistance marker, P00384) and CymR (HTH-type transcriptional regulator CymR, O33453). Assessments of changes in glycosylation were undertaken based on spectral counting of glycopeptide identification events with data visualization undertaken using ggplot2 [95] in R. To confirm the identity of glycoforms representative HCD and EThcD spectra were annotated with the aid of the Interactive Peptide Spectral Annotator tool (http://www.interactivepeptidespectralannotator.com/PeptideAnnotator.html) [96].

DIA-based proteomic analysis: DIA Datasets were searched using DIA-library free analysis within Spectronaut (version 17.6). Data files were searched against the *B. cenocepacia* K56-2 proteome (Uniprot accession: UP000011196, 7467 proteins, downloaded October 13th 2020) [97] and *B. cenocepacia* strain J2315 (Uniprot accession: UP000001035) [94], merging these proteomes enabling the matching of proteins to both J2315 and K56-2 accessions. Oxidation of Methionine was allowed as a variable modification, Carbamidomethyl was set as a fixed modification of Cysteine, and protease specificity was set to Trypsin. Protein quantitation was undertaken using MaxLFQ [98] based analysis. The precursor PEP was altered to 0.01 from the default 0.2 to improve quantitative accuracy, with all single peptide protein matches excluded. Statistical analysis was undertaken using Perseus [99] with missing values imputed based on the total observed protein intensities with a range of 0.3 σ and a downshift of 2.5 σ. Biological replicates were grouped together, and student t-tests were used to compare individual groups with a minimum fold change of +/- 1 considered for further analysis. Multiple hypothesis correction was undertaken using a permutation-based FDR approach allowing an FDR of 5%. Enrichment analysis using Fisher exact tests was undertaken in Perseus using Gene Ontology (GO) terms obtained from Uniprot (*B. cenocepacia* strain J2315 proteome: UP000001035) as well as against proteins previously reported as altered within K56-2 Δ*pglL,* K56-2 Δ*ogc or* K56-2 Δ*pglL*Δ*ogc* compared to K56-2 WT by Oppy *et al.* [63]. Data visualization was undertaken using ggplot2 [95] in R.

Data availability: All mass spectrometry data (RAW files, FragPipe outputs, Spectronaut outputs / experiment files, Rmarkdown scripts, and output tables) have been deposited into the PRIDE ProteomeXchange repository [100,101]. All PRIDE accession numbers, descriptions of the associated experiments and experiment types (DIA or DDA) are provided in **Supplementary Table 4**.

428 **Results:**

429 **Loss of *ogcA* and *ogcX* impacts viability of *B. cenocepacia***

430 To dissect the impact of individual *ogc* genes on viability, we established a rhamnose-
431 inducible vector pSCrhaB2 [64] containing the *ogc* cluster (pSCrhaB2-*ogc*) herein referred to as
432 p*ogc* (**Figure 1B**), and assessed its ability to restore glycosylation within *B. cenocepacia* Δ*ogc*
433 [47]. Using mass spectrometry-based proteomics, we confirmed the restoration of
434 glycosylation regardless of rhamnose induction and the absence of glycosylation within
435 Δ*ogc* containing pSCrhaB2 empty vector alone (**Figure 1C, Supplementary Table 6**). Notably,
436 we observed that the introduction of p*ogc* did not impact glycosylation levels within
437 *B. cenocepacia* WT regardless of induction state (**Figure 1C**). While glycosylation was
438 observed at comparable levels within strain/plasmid combinations containing endogenous
439 or plasmid complemented *ogc,* proteomic analysis demonstrates OgcX and OgcA were
440 below the limit of detection in the absence of rhamnose induction yet detectible upon
441 induction (**Figure 1D, Supplementary table 7**). With the identification that p*ogc* restored
442 glycosylation, we then sought to remove *ogcX* and *ogcA* within p*ogc* to assess the impact on
443 viability with *ogcI* / *ogcB* removed as additional controls (**Figure 1E**). To assess the impact of
444 *ogc* deletions on viability, we introduced plasmids into *B. cenocepacia* WT and Δ*ogc* by
445 conjugation assessing the recovery of viable colonies. Conjugation efficiency was not
446 impacted by the removal of *ogcA, B, I* or *X* within *B. cenocepacia* WT with comparable
447 cfu/mL observed; however, within Δ*ogc* conjugations of p*ogc*Δ*ogcX* and p*ogc*Δ*ogcA*
448 demonstrated dramatic reductions in recoverable cfu/mL (**Figure 1F**). These observations
449 support that the loss of either *ogcX* and *ogcA* within p*ogc* impacts viability in the absence of
450 chromosomally encoded *ogcX* and *ogcA*.

451

452 **Deleterious effects due to the loss of *ogcX* or *ogcA* are dependent on glycosylation**
453 **initiation**

454 The absence of effects on viability in response to the loss of the *ogc* [47,63] , yet the
455 requirement of *ogcA* / *ogcX* alone supports that if *O*-linked glycan biosynthesis is allowed to
456 proceed, it is deleterious after the addition of the second GalNAc, mediated by the OgcB [47].
457 If true, we reasoned that controlling the initiation of glycosylation via placing OgcI under

458 inducible control should render Δ*ogcA and* Δ*ogcX* viable. To assess this, we removed *ogcI*
459 and chromosomally re-introduced *ogcI* under rhamnose-inducible control within a miniTn7
460 integrative system (**Figure 2A, Supplementary Figure 1A and 1B**), generating Δ*ogcI* Tn7-
461 *ogcI.* Proteomic and glycoproteomic analysis confirmed the inducible control of *ogcI* as well
462 as the appearance of glycosylation upon the addition of rhamnose in this background
463 (**Supplementary Figure 2B and 2C**). Following verification of Δ*ogcI* Tn7-*ogcI,* we generated
464 viable mutations in *ogcX and ogcA* (Δ*ogcI*Δ*ogcX* Tn7-*ogcI* and Δ*ogcI*Δ*ogcA* Tn7-*ogcI*) as well
465 as *ogcB and ogcAB (*Δ*ogcI*Δ*ogcB* Tn7-*ogcI* and Δ*ogcI*Δ*ogcAB* Tn7-*ogcI*, **Supplementary Figure**
466 **3**). Consistent with the requirement of glycosylation initiation to drive deleterious effects,
467 spot plate assays in the presence of rhamnose revealed reduced growth within Δ*ogcI*Δ*ogcA*
468 Tn7-*ogcI* and Δ*ogcI*Δ*ogcX* Tn7-*ogcI* yet did not impact Δ*ogcI*Δ*ogcAB* Tn7-ogcI*,* Δ*ogcI*Δ*ogcB*
469 Tn7-ogcI or Δ*ogcI* Tn7-*ogcI* growth (**Figure 2B**). Quantification of colony size within strains
470 lacking *ogcX* or *ogcA* revealed a reduction in size to 10% of Δ*ogcI* Tn7-*ogcI*, Δ*ogcI*Δ*ogcB* Tn7-
471 *ogcI* and Δ*ogcI*Δ*ogcAB* Tn7-*ogcI* strains in response to induction (**Figure 2C**). Consistent with
472 these results, microtiter plate-based growth assays also revealed marked delays in the
473 growth kinetics of strains lacking *ogcX* or *ogcA* upon induction compared to Δ*ogcI* Tn7-*ogcI*
474 (**Supplementary Figure 4**). Importantly, across strains, quantification of glycosylation using
475 glycoproteomics supports that while rhamnose induction led to the restoration of
476 glycosylation within Δ*ogcI* Tn7-*ogcI,* no glycosylation was observable within strains lacking
477 *ogcA, B, X or AB* upon rhamnose induction (**Figure 2D, Supplementary Table 8**).

478 To support that the observed growth defects were *ogc*X and *ogc*A dependent, plasmid-
479 based complementation was undertaken. For OgcA complementation, two rhamnose
480 inducible vectors denoted as pSCrhaB2-*ogcA*-Met1 and pSCrhaB2-*ogcA*-Met2 corresponding
481 to variants differing in the two potential start codons of *ogcA* (**Supplementary Figure 5**),
482 herein referred to as p*ogcA*$_{Met1}$ and p*ogcA*$_{Met2}$ respectively, were generated. Upon induction
483 both p*ogcA*$_{Met1}$ and p*ogcA*$_{Met2}$ within Δ*ogcI*Δ*ogcA* Tn7-*ogcI* restored colony size to
484 comparable levels observed within Δ*ogcI* Tn7-*ogcI* (**Figure 3A**). Interestingly, Δ*ogcI*Δ*ogcA*
485 Tn7-*ogcI* carrying the empty vector pSCrhaB2 was unable to grow in the presence of plasmid
486 antibiotic selection conditions upon induction even with reduced rhamnose induction levels
487 (**Supplementary Figure 6A**). Proteomic and glycoproteomic analysis confirms the induction
488 of OgcA and restoration of glycosylation within Δ*ogcI*Δ*ogcA* Tn7-*ogcI* containing either

489 p*ogcA*$_{Met1}$ or p*ogcA*$_{Met2}$ in a rhamnose dependent manner (**Figure 3B-C, Supplementary**
490 **Table 9 and 10**). Consistent with spot plate assays proteomic and glycoproteomic analysis of
491 Δ*ogcI*Δ*ogcA* Tn7-*ogcI* containing pSCrhaB2 was unable to be assessed under rhamnose
492 induction due to loss of viability. To complement *ogcX,* we generated a modified pMLBAD
493 vector [70] placing *ogcX* expression under cumate inducible control generating pCumate-*ogcX-*
494 *his*, herein referred to as p*ogcX* as well as a control plasmid containing GFP, pCumate-sfGFP
495 here in referred to as p*sfGFP*. Akin to *ogcA* complementation, the introduction of p*ogcX* into
496 Δ*ogcI*Δ*ogcX* Tn7-*ogcI* restored colony size compared to p*sfGFP* following rhamnose
497 induction with the presence of p*ogcX,* regardless of cumate induction, sufficient to relieve
498 the deleterious effects of glycosylation initiation (**Figure 3D**). As with Δ*ogcI*Δ*ogcA* Tn7-*ogcI*
499 carrying pSCrhaB2, loss of viability of Δ*ogcI*Δ*ogcX* Tn7-*ogcI* carrying p*sfGFP* was observed in
500 the presence of plasmid antibiotic selection conditions and rhamnose induction
501 (**Supplementary Figure 6B**). Glycoproteomic analysis confirmed the restoration of
502 glycosylation of Δ*ogcI*Δ*ogcX* Tn7-*ogcI* containing p*ogcX* in a rhamnose-dependent manner
503 (**Figure 3E, Supplementary Table 11**) with proteomic analysis supporting the production of
504 OgcX in the absence of cumate (**Figure 3F, Supplementary Table 12**) consistent with low
505 level constitutive expression of OgcX from p*ogcX*. As observed within *ogcA*
506 complementation, proteomic/glycoproteomic analysis of Δ*ogcI*Δ*ogcX* Tn7-*ogcI* containing
507 p*sfGFP* was unable to be assessed under rhamnose induction due to loss of viability (**Figure**
508 **3E/F**). Combined, these complementation assays support that the loss of *ogcA* and *ogcX*
509 drive the deleterious effects on the viability of *B. cenocepacia* upon glycosylation initiation.

510

511 **Proteomic analysis reveals loss of *ogcX* or *ogcA* drives alterations within the membrane**
512 **proteome**

513 Our initial proteomic characterisations (**Figure 1D, 3A, 3F**) revealed variability in tracking
514 proteins of the OGC; thus, to improve the depth and reproducibility of protein
515 quantification of these proteins, we turned to the use of Data-Independent Acquisition (DIA)
516 based proteomics [102,103]. To understand the proteomic changes uniquely driven by loss of
517 *ogcX* and *ogcA* we compared the proteome of four strains Δ*ogcI* Tn7-*ogcI,* Δ*ogcI*Δ*ogcA* Tn7-
518 *ogcI,* Δ*ogcI*Δ*ogcB* Tn7-*ogcI and* Δ*ogcI*Δ*ogcX* Tn7-*ogcI* under both rhamnose induced and
519 non-induced conditions. Using DIA proteomic analysis, all five proteins of the OGC were

520 observed allowing the confirmation of the expected loss of OGC proteins (**Supplementary**
521 **Figure 7, Supplementary Table 13**). Across strains, a total of 3748 proteins were identified,
522 with ~90% identified with >2 unique peptides in each biological replicate (**Supplementary**
523 **Figure 8A**). Principal component analysis revealed distinct clustering for each biological
524 group, with the Δ*ogcI*Δ*ogcA* Tn7-*ogcI* and Δ*ogcI*Δ*ogcX* Tn7-*ogcI* strains separating along PC1
525 upon induction supporting the loss of these genes leading to similar overall proteomic
526 effects when glycosylation is initiated (**Figure 4A**). Examination of the protein alterations
527 between non-induced and induced conditions revealed that induction resulted in significant
528 changes (defined as >2-fold difference and -log10(p-value) > 2) within strains lacking *ogcX*
529 and *ogcA* while relatively few alterations were observed within Δ*ogcI*Δ*ogcB* Tn7-*ogcI* and
530 Δ*ogcI* Tn7-*ogcI* (**Figure 4B**). Across the alterations observed in Δ*ogcI*Δ*ogcX* Tn7-*ogcI* and
531 Δ*ogcI*Δ*ogcA* Tn7-*ogcI*, 722 proteins were differentially impacted in both, with Δ*ogcI*Δ*ogcX*
532 Tn7-*ogcI* exhibiting the highest number of overall protein alterations (**Figure 4C**). Notably,
533 the protein alterations upon induction within Δ*ogcI*Δ*ogcX* Tn7-*ogcI* and Δ*ogcI*Δ*ogcA* Tn7-
534 *ogcI* were highly similar, demonstrating significant co-enrichment (Fisher exact test
535 Benjamini-Hochberg corrected *p*-value = $8.20*10^{-204}$, **Supplementary Table 14 and**
536 **Supplementary Figure 8B**) with these alterations also being highly correlative (Pearson
537 correlation: 0.81, **Figure 4E**). To assess the overall patterns within the observed protein
538 alterations, Gene Ontology (GO) enrichment was undertaken on the proteome alterations
539 observed within Δ*ogcI*Δ*ogcX* Tn7-*ogcI,* revealing an over-representation of membrane-
540 associated protein classes (**Figure 4D, Supplementary Table 14**). This over-representation
541 corresponds to the increased abundance of the observable membrane proteome in both
542 Δ*ogc*IΔ*ogc*X Tn7-ogcI and Δ*ogc*IΔ*ogc*A Tn7-ogcI upon induction (**Figure 4E**). Examination of
543 the increased membrane proteins (**Figure 4F**) confirms the induction of OgcI (BCAL3118), as
544 well as increases in functionally diverse membrane proteins, including BCAM1996 (a
545 homolog of the cell envelope integrity protein CreD), transporters such as
546 BCAL1079/BCAL1081 and BCAL1511/BCAL1512, outer membrane efflux proteins such as
547 BCAL3514, BCAS0014, and BCAL1456, as well as membrane proteins of unknown functions,
548 including BCAL2191 and BCAM1247. It should be noted that the proteomic alterations
549 observed during induction within Δ*ogc*IΔ*ogc*X Tn7-ogcI and Δ*ogc*IΔ*ogc*A Tn7-ogcI
550 demonstrate a partial overlap within proteins previously reported to be impacted by the
551 loss of glycosylation (**Supplementary Figure 9**) [63]. Combined, DIA proteomic analysis

552 supports disruptions within *ogc*X and *ogc*A leads to widespread proteomic alterations,
553 characterized by a dramatic increase in the membrane proteome when glycosylation is
554 initiated.

555

556 **Loss of *ogcA* and *ogcX* impacts membrane integrity and permeability of *B. cenocepacia***

557 Given the dramatic membrane proteomic alterations in response to the loss of *ogcX* and
558 *ogcA* upon induction, we hypothesised that these alterations suggests the loss of membrane
559 integrity as noted during the inhibition of several Wzx-dependent glycan pathways [4,6,7,34,104].
560 To assess membrane integrity, we assayed the impact of membrane stress (0.01% SDS)
561 using spot plate assays revealing increased sensitivity of Δ*ogcI*Δ*ogcA* Tn7-*ogcI* and
562 Δ*ogcI*Δ*ogcX* Tn7-*ogcI* upon glycosylation initiation compared to Δ*ogcI* Tn7-*ogcI,* Δ*ogcI*Δ*ogcB*
563 Tn7-*ogcI or* Δ*ogcI*Δ*ogcAB* Tn7-*ogcI* strains (**Figure 5A**). In contrast, osmotic stress (2% NaCl)
564 spot plate assays revealed adverse impacts on all strains in the absence of induction, yet
565 only *ogcX* and *ogcA* deletion strains failed to show improved viability following glycosylation
566 initiation (**Figure 5A**). Microtiter plate-based growth assays recapitulated these observations
567 with the strains lacking *ogcX* and *ogcA* demonstrating alterations in growth kinetics in the
568 presence of 0.01% SDS or 2% NaCl (**Supplementary Figure 10**). Consistent with the loss of
569 viability being driven by the absence of *ogcX* and *ogcA* complementation ameliorated the
570 growth defects in the presence of 0.01% SDS or 2% NaCl (**Figure 5B & C)**. These observations
571 support the loss of membrane integrity within Δ*ogcX* and Δ*ogcA* backgrounds yet to directly
572 assess membrane permeability in response to glycosylation initiation, we undertook
573 Hoechst 33342 and N-phenyl-1-naphthylamine (NPN) fluorescent-based permeability
574 assays. Utilising Hoechst 33342, a fluorescent DNA binding dye, we evaluated DNA binding
575 revealing enhanced fluorescence within Δ*ogcX* and Δ*ogcA* backgrounds upon glycosylation
576 initiation, yet minimal alterations in Δ*ogcI* Tn7-*ogcI,* Δ*ogcI*Δ*ogcB* Tn7-*ogcI or* Δ*ogcI*Δ*ogcAB*
577 Tn7-*ogcI* (**Figure 5D**). Similarly, NPN uptake assays, which monitor dye partitioning into
578 membranes [83], revealed increased fluorescence in Δ*ogcI*Δ*ogcX* Tn7-*ogcI* and Δ*ogcI*Δ*ogcA*
579 Tn7-*ogcI* upon induction, supporting increased membrane permeability (**Figure 5E**,
580 **Supplementary Figure 11**) with complementation of Δ*ogcI*Δ*ogcX* Tn7-*ogcI* and Δ*ogcI*Δ*ogcA*
581 Tn7-*ogcI* reversing membrane permeability (**Supplementary Figure 12**). Combined, these
582 findings support the absence of *ogcX* and *ogcA* upon glycosylation initiation compromises

583 the *B. cenocepacia* envelope, leading to sensitisation to stressors and membrane
584 permeability.

585

586 **Loss of *ogcA* and *ogcX* enhances sensitivity of *B. cenocepacia* to antimicrobials**

587 The observations that the loss of *ogcX* and *ogcA* leads to widespread impacts on the
588 *B. cenocepacia* membrane highlight the potential for these effects to be exploited to
589 potentiate antimicrobial agents. In line with this, recent transposon studies have suggested
590 that mutations within the *ogc* alter susceptibility to β-lactam antibiotics; however,
591 validation of these effects using CRISPRi resulted in only modest recapitulation of
592 sensitization [61]. Given the growth defects observed in response to induction under plasmid
593 selection conditions (**Figure 3A, 3D and Supplementary Figure 6**), this suggests the
594 enhanced sensitivity of strains lacking *ogcX* and *ogcA* to trimethoprim. Thus, we assessed
595 the impact of antimicrobial agents including trimethoprim, tetracycline, ceftazidime,
596 chlorhexidine and rifampicin on glycosylation inducible strains. Utilising broth dilution
597 assays, changes in antimicrobial sensitivity were observed in strains lacking *ogcX* and *ogcA*
598 upon induction yet were modest in magnitude corresponding to a 1- to 2-fold decrease in
599 the minimal inhibitory concentrations (MIC) of trimethoprim and ceftazidime
600 (**Supplementary Figure 13 and Supplementary Table 5**). To improve the detection of
601 alterations in antimicrobial sensitivity, we assessed the impact of antimicrobial agents at or
602 below the broth dilution-defined MICs using spot assays. Utilising this approach, upon
603 induction, strains lacking *ogcX* and *ogcA* were observed to show enhanced sensitivity to
604 tetracycline, rifampicin, trimethoprim and ceftazidime compared to Δ*ogcI*Δ*ogcB* Tn7-*ogcI*
605 and Δ*ogcI* Tn7-*ogcI* (**Figure 6**). Interestingly, for both trimethoprim and ceftazidime, all
606 strains showed reduced growth without induction, yet the growth of Δ*ogcI*Δ*ogcB* Tn7-*ogcI*
607 and Δ*ogcI* Tn7-*ogcI* was improved upon induction (**Figure 6**). Combined, these findings
608 support the loss of *OGC* genes sensitise *B. cenocepacia* to several antimicrobial agents with
609 these impacts most pronounced for strains lacking *ogcX* or *ogcA* upon initiation of
610 glycosylation.

611

612 **Expression of UppS and OgcX improves the viability of *B. cenocepacia* in response to *ogc***
613 **biosynthesis blockages.**

614 As the deletion of *ogcA* and *ogcX* leads to deleterious effects upon glycosylation initiation,
615 we sought to further support the role of Und-P/Und-PP sequestration in driving these
616 effects. We reasoned that modulating Und-P precursor levels or enhancing glycan
617 intermediate translocation would counteract Und-P/Und-PP sequestration. To probe this,
618 we overexpressed undecaprenyl pyrophosphate synthase (UppS), the *de novo* synthase
619 responsible for generating Und-P, which has been previously shown to relieve Und-P
620 sequestration (**Figure 7A**) [7,105]. Utilising cumate-inducible vectors containing the two
621 putative annotated UppS enzymes of *B. cenocepacia* K56-2, BCAL2087 and BCAM2067
622 within the vectors p*BCAL2087* and p*BCAM2067* respectively, we assessed the impact of
623 UppS overexpression in the absence of *ogcA* and *ogcX* with glycosylation initiation. Within
624 Δ*ogcI*Δ*ogcA* Tn7-*ogcI* and Δ*ogcI*Δ*ogcX* Tn7-*ogcI*, the induction of p*BCAL2087* partially
625 alleviated reductions observed within Δ*ogcA* and Δ*ogcX*, while p*BCAM2067* only restored
626 viability within Δ*ogcI*Δ*ogcA* Tn7-*ogcI* (**Figure 7B**). These observations support the partial
627 repression of growth defects upon induction of UppS. To assess if enhancing glycan
628 translocation restores growth, we introduced *pogcX* into Δ*ogcI*Δ*ogcA* Tn7-*ogcI* which
629 improved growth upon the initiation of glycosylation (**Figure 7C**). To probe the impact of
630 OgcX overexpression on membrane integrity spot assays were undertaken revealing the
631 amelioration of growth defects within Δ*ogcI*Δ*ogcA* Tn7-*ogcI* compared to the control vector
632 p*sfGFP* (**Figure 7D/E**). Surprisingly, while *pogcX* improved resistance to membrane stresses
633 in Δ*ogcI*Δ*ogcA* Tn7-*ogcI* in response to 0.01% SDS (**Figure 7D**) we noted reduced viability
634 within Δ*ogcI*Δ*ogcB* Tn7-*ogcI* in response to salt and SDS stress compared to the control
635 vector p*sfGFP* (**Figure 7D/E**). To confirm the overexpression of OgcX allowed the
636 translocation of incomplete *O*-linked glycans we undertook glycoproteomic analysis
637 confirming both enhanced glycosylation within inducible strains and the appearance of
638 truncated glycans within Δ*ogcI*Δ*ogcA* Tn7-*ogcI* and Δ*ogcI*Δ*ogcB* Tn7-*ogcI* (**Figure 7F,**
639 **Supplementary Table 15 and 16**). Manual inspection of glycopeptide assignments within
640 Δ*ogcI*Δ*ogcA* Tn7-*ogcI* confirms the identity of these glycosylation events as corresponding to
641 the modification of peptides with $HexNAc_2$ glycans (**Figure 7G**). Of note, while glycopeptide
642 analysis suggested the presence of both $HexNAc_2$ and HexNAc modified peptides within

643 Δ*ogcI*Δ*ogcB* Tn7-*ogcI* (**Figure 7F**) manual inspection of glycopeptide spectra demonstrate
644 the miss assignment of glycopeptides possessing multiple individual glycosylation events as
645 $HexNAc_2$ events (**Supplementary Figure 14**). Combined, these data demonstrate that both
646 modulating UppS activity and enhancing glycan translocation of $HexNAc_{2,}$ but not HexNAc,
647 alleviates the growth defects associated with initiating glycosylation in strains defective in
648 completing the Burkholderia O-linked glycan.

649

650 **Modulation of early steps in *ogc* biosynthesis are also detrimental to *B. cenocepacia***
651 **viability**

652 Finally, as changes driven by *ogc* perturbations were detrimental we questioned if shifting
653 the equilibrium of the Und-P/Und-PP pool associated with the *ogc* alone would also impact
654 viability. To probe this, we overexpressed components of the *ogc* within the parental
655 *B. cenocepacia* K56-2 background and assess viability utilising spot assays. Introduction of
656 rhamnose inducible vectors containing *ogcI* (p*ogcI*), *ogcB* (p*ogcB*), *ogcA* (p$ogcA_{Met1}$) as well
657 as the vector p$ogcAB_{Met1}$, *which* allows the expression of both *ogcA* and *ogcB,* revealed
658 induction of p*ogcI* and p*ogcB* resulted in reduced viability, while the overexpression of
659 *ogcA*(p*ogcA*), *ogcAB* (p*ogcAB*), and the complete *ogc* (p*ogc*) showed no impact on viability
660 (**Figure 8**). Critically, complementation of *B. cenocepacia* Δ*ogcAB,* Δ*ogcB* and Δ*ogcI* with
661 p$ogcAB_{Met1}$, p*ogcB* and p*ogcI* induced with 0.05% rhamnose restored glycosylation,
662 confirming the functionality of these constructs (**Supplementary Figure 15 to 17,**
663 **Supplementary Table 17 to 22**). These observations support that the overexpression of
664 early steps in *O*-linked glycan biosynthesis, OgcI and OgcB, appear to impact viability, yet
665 these effects can be alleviated in the case of *ogcB* by co-expression of *ogcA*. Combined,
666 these observations support alterations in early steps in *O*-linked glycan biosynthesis
667 modulate *ogc*-associated viability supporting the sensitivity of the Und-P/Und-PP pool to
668 sequestration from non-physiological expression levels of *ogc* proteins.

669 **Discussion:**

670 *Burkholderia O*-linked glycosylation, mediated by the *ogc* and *pglL* [47,59], are highly conserved
671 at the pathway and glycan composition levels [45-47]. While previous work demonstrated the
672 requirement of the *ogc* for the generation of the trisaccharide used for glycosylation [47], a
673 deeper understanding of how glycan fidelity is controlled, as well as the impact of *ogcA* and
674 *ogcX* on *B. cenocepacia* has not been assessed. In line with the growing recognition of the
675 impact of Und-P/ Und-PP sequestration by dead-end intermediates of O-antigens [6,11],
676 capsule [35], cell wall teichoic acids [106,107] and the ECA [7,10] glycans, we demostrate that
677 blocking *ogc* also lead to sequestration of the Und-P/ Und-PP pool. Critically, this work
678 highlights that in line with previous studies on Wzx-dependent glycan pathways [3,4,10,27], the
679 *B. cenocepacia O*-linked glycosylation pathway appears highly selective for its complete
680 cognate glycan. This observation sheds light on the near-exclusive presence of the observed
681 Gal–GalNAc$_2$ structure decorating glycoproteins within all *Burkholderia* glycoproteomic
682 studies to date [46,47,59,88,108,109] and the mechanism responsible for glycan selectivity.

683 The conservation of the *Burkholderia O*-linked glycan makes this glycosylation system
684 unique among characterised bacterial protein glycosylation systems to date, including the
685 *O*-linked glycosylation systems of *Acinetobacter* [110-112] and *Neisseria* [40,58,113], as well as the *N*-
686 linked glycosylation systems of *Campylobacter* [38,39] where extensive glycan diversity has
687 been observed. While the conservation of glycans in the context of protein glycosylation
688 systems appears atypical, the conservation of glycan biosynthesis across species, or even
689 genera, has previously been noted, as in the case of the ECA [114,115]. For the ECA, it has been
690 suggested that the invariance of this oligosaccharide underpins its importance to
691 Enterobacterales physiology [115]. While the function of *Burkholderia O*-linked glycosylation is
692 still unknown, this work raises a critical question on the importance of the cognate glycan in
693 glycosylation. Despite the identification of *B. cenocepacia* protein glycosylation over a
694 decade ago, we have yet to identify a specific function for glycosylation, nor have individual
695 glycosylation events been identified that require glycosylation for functionality [59,63,109]. As
696 demonstrated for other Wzx, non-native substrates can be translocated under heightened
697 levels of flippase expression [14-16] and consistent with this we demonstrate that
698 overexpression of OgcX enhances the translocation of non-cognate *ogc* structures (**Figure**
699 **7F/G**). These overexpression studies support the role of OgcX as a flippase and confirms the

700 function of OgcA as the glycosyltransferase responsible for adding the final Gal residue of
701 the *O*-linked trisaccharide. Importantly this ability to enhance translocation within
702 Δ*ogcI*Δ*ogcA* Tn7-*ogcI* allows us to demonstrate that poor translocation efficiency appears to
703 underpin the detrimental effects observed from the loss of OgcA (**Figure 7B-E**). However, we
704 observe that translocation of a single HexNAc, as seen in the case of Δ*ogc*IΔ*ogc*B Tn7-*ogcI*
705 appears to be detrimental to *B. cenocepacia* in response to salt and SDS stressors (**Figure**
706 **7D/E**) suggesting that glycosylation with HexNAc alone may be insufficient for optimal *B.*
707 *cenocepacia* physiology in response to membrane stressors. Thus, this work provides
708 experimental confirmation of the roles of OgcX as well as OgcA, highlights how *O*-linked
709 glycan fidelity is controlled and supports the importance of glycosylation with specific glycan
710 structures within *B. cenocepacia* for membrane stress resistance.

711 Our observations of deleterious effects in response to the loss of *ogcX* (**Figure 1, 2 & 3**)
712 suggest the previously reported Δ*ogcX* isolate within *B. cenocepacia* [47] likely possessed an
713 uncharacterised suppressor mutation. As noted previously, suppressor mutations can
714 rapidly emerge upon Und-P/Und-PP sequestration [9,33,34] with the emergence of a potential
715 suppressor mutation highlighted as the potential source of confounding results associated
716 with defining the function of the WzxE flippase within *E. coli* K-12 [10]. While we were unable
717 to obtain the previously reported Δ*ogcX* isolate the observation that low-level glycosylation
718 of a truncated glycan of a single HexNAc residue was observed within this strain [47], suggests
719 a potential disruption within the *O*-linked glycosylation system. In contrast to previous
720 results, our observation of the requirement of OgcX for *O*-glycosylation supports that this
721 flippase is indispensable within *B. cenocepacia* for translocation of the *O*-linked glycan into
722 the periplasmic space. Interestingly, not all flippases are indispensable as has been noted
723 within *E. coli* K-12, where some redundancy exists in the ability of ECA to be mobilised to
724 the periplasm by the O-antigen (Wzx_{O16}) or colanic acid (WzxC) flippases [116]. Our analysis of
725 glycosylation in the absence of *ogcX* (**Figure 2D**) is consistent with a lack of functional
726 redundancy for the cognate *O*-linked glycan by the remaining Wzx flippases of
727 *B. cenocepacia.* Within *B. cenocepacia* K56-2, previous analysis has highlighted the presence
728 of at least five putative Wzx flippases with similar functional indispensability observed for
729 the peptidoglycan flippase $murJ_{Bc}$ (BCAL2764) [117]. Thus, these findings support that OgcX is

730 the sole flippase required for translocation of the *O*-linked glycan, and alternative flippases
731 are not functionally redundant for this glycan in *B. cenocepacia.*

732 We have previously reported the inability to generate Δ*ogcA* within *B. cenocepacia* [47], yet
733 disruptions of *ogcA* were recently suggested to be tolerated [61]. Our data assessing the loss
734 of *ogcA* using plasmid-based complementation (**Figure 1**) as well as strains with inducible
735 control of glycosylation (**Figure 2 to 7**) supports that, akin to *ogcX*, the loss of *ogcA* is
736 deleterious within *B. cenocepacia*. Previously, putative Δ*ogcA* candidates were observed
737 within high-density transposon libraries yet *ogcA* CRISPRi silencing failed to recapitulate the
738 resulting phenotypes associated with Δ*ogcA* [61]. As such, we suggest that the Δ*ogcA* reported
739 within prior work may contain unexpected secondary mutations or that the presence of
740 transposons within *ogcA* may have adversely affected the expression of neighbouring genes
741 of the *ogc*. While transposon libraries coupled with sequencing provide a robust means to
742 assess gene function at a genomic scale [118], it is recognised that this approach can lead to
743 inactivation or polar effects in neighbouring genes [119,120]. Furthermore, the enrichment of
744 transposon junctions prior to sequencing [118] does not allow the assessment of unlinked
745 potential suppressor or inactivation events, which may restore variability even in the
746 presence of insertions into conditionally essential genes. Of note within our work, the
747 utilisation of proteomics allowed the assessment of *ogcA,* ogc*X,* and ogc*B* mutagenesis,
748 revealing neighbouring *ogc* proteins are unaffected by the removal of these genes
749 (**Supplementary Figure 7**). Considering our findings, in addition to prior transposons studies
750 of *B. cenocepacia* and *Burkholderia pseudomallei* that assign *ogcA* as essential [60,62], this
751 supports the assignment of *ogcA* as conditionally essential.

752 The observation that both *ogcA* and *ogcX* appear conditionally essential is consistent with a
753 growing body of work highlighting the detrimental impacts of blocking Und-P/PP
754 biosynthetic pathways [6,7,11]. As with previous studies on the deleterious impacts of Und-
755 P/PP sequestration, the use of inducible systems [10,11,14] provided a tractable way to explore
756 the roles of *ogcA*/*ogcX* while limiting potential confounding effects from the emergence of
757 suppressors. The inducible deleterious effects from the loss of *ogcA* and *ogcX* (**Figure 2**)
758 support fouling of the Und-P/PP pool with complementation confirming the restoration of
759 glycosylation as well as suppression of growth defects by the re-introduction of *ogcX* / *ogcA*
760 (**Figure 3 and 5**). Interestingly, within this work, we noted that while the introduction of

761 plasmid variants lacking *ogcA/X* were unable to be recovered from *B. cenocepacia* Δ*ogc*
762 rhamnose inducible strains lacking *ogcA/X* were viable although exhibited reduced growth
763 rates (**Figure 2, Supplementary Figure 4**). While the viability of inducible Δ*ogc*IΔ*ogc*A Tn7-
764 ogcI *and* Δ*ogc*IΔ*ogc*X Tn7-ogcI strains was essential for allowing proteomic (**Figure 4**) and
765 phenotypic assessments (**Figure 5, 6 and 7**), this does suggest the overall restoration of
766 glycosylation mediated by Tn7-rha-*ogcI* may be reduced compared to wild type
767 *B. cenocepacia,* reducing the magnitude of the effect of sequestration on the Und-P/PP
768 pool. In line with this, we noted higher overall glycosylation levels, as determined by
769 identified glycopeptides, within wildtype *B. cenocepacia* (**Figure 1C**) compared to the
770 observed levels within glycosylation inducible strains (**Figure 2D, 3C, 3F and 7D**) consistent
771 with an overall reduced glycosylation capacity. Regardless, the ability to demonstrate
772 changes in membrane permeability and stress sensitivity (**Figures 5 and 6**) highlights the
773 importance of *O*-linked glycan completion for *B. cenocepacia* physiology as well as allowed
774 the assessment of antibiotic sensitisation previously suggested for Δ*ogcA* [61]. Our work
775 demonstrates that upon initiation of glycosylation both Δ*ogcA and* Δ*ogcX* become sensitised
776 to clinically important antibiotics including tetracycline, rifampicin, trimethoprim as well as
777 ceftazidime (**Figure 6**). This enhanced sensitivity also reconciles the differences we observe
778 between experiments undertaken using plasmids (**Figure 1F, 3A, 3D, 5B, 5C, 7B, 7D and**
779 **Supplementary Figure 6**) compared to inducible strains alone (**Figure 2B and 5A**) supporting
780 that the antibiotic selection required to maintain plasmids exacerbates the observed
781 viability defect within Δ*ogcA and* Δ*ogcX strains*. It should be noted that the observation that
782 inhibiting *ogcA* or *ogcX* can modulate antibiotic sensitisation suggests targeting the *ogc* may
783 be a potent way to sensitise *Burkholderia* to antibiotics. The concept of modulating the Und-
784 P/PP pool to sensitise *B. cenocepacia* has been previously explored by the depletion of *dxr*
785 (BCAL2085) [121], which directly contributes to the precursors required for UppS-mediated *de*
786 *novo* synthesis of Und-P [1,122]. Thus, fouling of the Und-P/PP pool through inhibition of OgcX
787 or OgcA may be an attractive approach for drug re-sensitisation.

788 Previous studies have noted that the inhibition of peptidoglycan biosynthesis is likely the
789 key defect responsible for the deleterious effects of Und-P/PP fouling [6,7,105]. Consistent with
790 this our DIA proteomic analysis reveals an increase in several proteins associated with
791 peptidoglycan upon initiation of glycosylation within Δ*ogcA/X* strains including BCAL0310

792 (*murA*), BCAL3412 (*mtgA*), BCAL3463 (*fts*W) and BCAL2777 *a* putative N-acetylmuramoyl-L-
793 alanine amidase (**Supplementary Table 13, Supplementary Figure 18**). Interestingly, among
794 the altered membrane proteins, one of the most significant changes observed within Δ*ogcA*
795 and Δ*ogcX* corresponds to a >30-fold increase in BCAM1996 (CreD, **Figure 4F**). Within
796 *Pseudomonas aeruginosa* CreD is known to be associated with sensing changes in
797 peptidoglycan synthesis being potently transcribed in response to perturbations in
798 peptidoglycan binding proteins [123] and suggested to be important for peptidoglycan Und-
799 P/Und-PP recycling [124]. Similarly, within *Stenotrophomonas maltophilia* CreD has also been
800 shown to be critical for envelope integrity and maintaining cell morphology [125]. The
801 increased abundance of CreD in response to glycosylation initiation within Δ*ogc*IΔ*ogc*A Tn7-
802 ogcI *and* Δ*ogc*IΔ*ogc*X Tn7-ogcI may suggest a more general role for CreD in Und-P/Und-PP
803 recycling. Of the proteomic alterations observed it is notable that the proteome changes
804 observed within Δ*ogc*IΔ*ogc*A Tn7-ogcI and Δ*ogc*IΔ*ogc*X Tn7-ogcI are similar yet more
805 extensive than the proteomic changes observed from the loss of glycosylation alone
806 (**Supplementary Figure 9**) [63]. These observations support that blocking *ogc* biosynthesis
807 induces extensive and pleiotropic effects, beyond the changes seen from the loss of protein
808 glycosylation alone, including evidence of changes in peptidoglycan biosynthesis which are
809 consistent with Und-P/PP fouling.

810 In this study, it is noteworthy that for the overexpression of the putative UppS enzymes only
811 BCAL2087 was able to alleviate the growth defects associated with glycosylation initiation in
812 both the Δ*ogcA* and Δ*ogcX* backgrounds yet BCAM2067 only partially restored the viability
813 of Δ*ogcI*Δ*ogcA* Tn7-*ogcI* (**Figure 7B**). While the exact cause of this difference is unclear, it is
814 important to note that the Und-P/PP pool is not a homogeneous pool of polyisoprenyl lipids
815 [126]. It is possible that the assigned UppS enzymes contribute different polyisoprenyl lipids,
816 which influence the Und-P/PP pool and lead to changes in tolerance to Und-PP
817 intermediates, however, this is speculative, and the exact cause of this difference is
818 unknown. Consistent with changes in the Und-P/PP pool impacting viability our analysis of
819 individual *ogc* components reveals OgcI and OgcB alone as sufficient to inhibit growth when
820 overexpressed within *B. cenocepacia* (**Figure 8**). These proteins do not themselves impact
821 growth within *E. coli* (**Supplementary Figure 19**) and when induced with 0.05% rhamnose
822 restore glycosylation within *B. cenocepacia* Δ*ogcB* and Δ*ogcI* (**Supplementary Figure 16 and**

823 **17**). Thus, this reduced viability observed upon induction of OgcI and OgcB supports that
824 increasing the proportion of early-stage intermediates in *ogc* biosynthesis leads to the
825 sequestration of the Und-PP/P pool. In line with this model, the overexpression of OgcA
826 with OgcB was found to relieve toxicity, supporting the importance of adequate enzyme
827 capacities in meeting the demands during *ogc* biosynthesis. It should be noted a caveat of
828 our model is the assumption that the products of the *ogc* solely supply glycan units used for
829 protein glycosylation, yet whether this is the case is unknown. As noted within other glycan
830 biosynthesis pathways both glycan intermediates as well as complete glycan units may be
831 incorporated into different glycoconjugates [114,115]. Previous studies of *O*-linked glycosylation
832 systems have demonstrated that glycans used for glycosylation may be derived from several
833 Und-P-dependent biosynthesis pathways, such as the O-antigen in *Pseudomonas aeruginosa*
834 [127,128] and capsule pathways within the *Moraxellaceae* [129,130]. In light of this, while the *ogc* is
835 sufficient and required for protein glycosylation [47] and we show the modulation of *ogc*
836 intermediates impact viability, it is currently unclear if this pathway contributes solely to
837 protein glycosylation, which impacts the interpretation of these findings.

838 In conclusion, this work demonstrates that the loss of *ogcA/X* within *B. cenocepacia* results
839 in detrimental impacts on viability, membrane permeability and the proteome, which
840 appears to sensitise strains to membrane stresses including clinically useful antibiotics. This
841 work highlights that akin to the impacts of glycan biosynthesis blockages observed in O-
842 antigens [6,9] and the ECA [7,10], modulating or blocking the generation of *ogc* intermediates
843 appears to lead to sequestration of the Und-P/PP pool within *B. cenocepacia.* These findings
844 not only advance our mechanistic understanding of how glycan fidelity is maintained for
845 Burkholderia *O*-linked protein glycosylation but the therapeutic potential of targeting steps
846 in this pathway.

Acknowledgements:

N.E.S was supported by an Australian Research Council (ARC) Future Fellowship (FT200100270), an ARC Discovery Project Grant (DP210100362) and a National Health and Medical Research Council Ideas grant (2018980). We thank the Melbourne Mass Spectrometry and Proteomics Facility of The Bio21 Molecular Science and Biotechnology Institute for access to MS instrumentation. We thank Nicholas Coleman for sharing the plasmid pUS250-sfGFP and Erin Garcia for sharing the plasmid pFlptet.

AUTHOR CONTRIBUTION STATEMENT:

Leila Jebeli: Investigation, Validation, Visualization, Writing - Original Draft, Formal analysis; **Taylor A. McDaniels:** Investigation, Visualization, Formal analysis, Supervision; **Duncan T. T. Ho:** Investigation, Visualization, Formal analysis; **Hamza Tahir:** Investigation, Resources; **Nicholas L. Kai-Ming:** Investigation, Visualization; **Molli Mcgaw:** Investigation, Resources; **Kristian I. Karlic:** Software, Formal analysis, Visualization; **Jessica M. Lewis:** Supervision, Investigation, Visualization; **Nichollas E. Scott:** Conceptualization, Visualization, Investigation, Formal analysis, Supervision, Writing - Review & Editing, Funding acquisition.

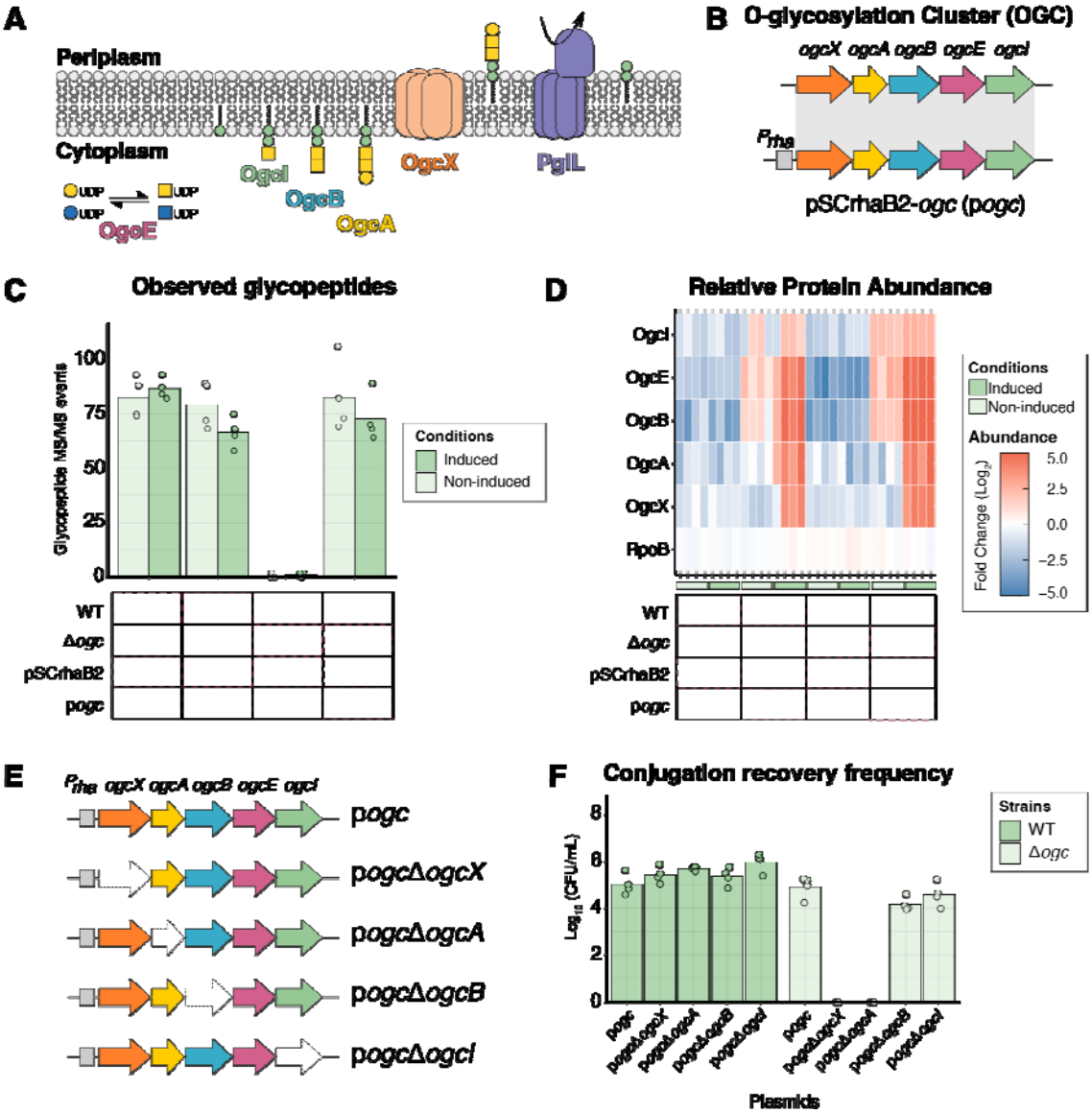

Figure 1. Loss of *ogc*X and *ogc*A impacts viability of *B. cenocepacia* Δ*ogc*. A) Diagram of the *O*-glycosylation biosynthesis pathway in *Burkholderia* species [47]. *O*-glycosylation biosynthesis involves the stepwise construction of a conserved trisaccharide composed of Gal-GalNAc$_2$ by the glycosyltransferases, OgcI, OgcB and OgcA, with the nucleotide-sugar donors UDP-GalNAc and UDP-Gal generated by the epimerase OgcE. The resulting trisaccharide is then thought to be translocated across the inner membrane by the putative flippase, OgcX. Once in the periplasm, the glycans can be transferred to proteins by the oligosaccharyltransferase, PglL. **B)** Graphic representation of the genetic organization of the *ogc* cluster (*ogc*X, A, B, E and I assigned as BCAL3114–BCAL3118 within *B. cenocepacia* J2315) and its integration into the rhamnose-inducible vector pSCrhaB2, resulting in the

876 generation of the pSCrhaB2-*ogc* (p*ogc*). **C-D)** Quantification of glycopeptide and protein
877 levels encoded by the *ogc* cluster identified from whole cell proteomic analysis of
878 *B. cenocepacia* WT and Δ*ogc* containing either pSCrhaB2 or p*ogc* with and without induction
879 with 1% rhamnose (n=4). **E)** Graphic representation of p*ogc* mutagenesis removing *ogc*X,
880 *ogc*A, *ogc*B and *ogc*I. **F)** Conjugation of p*ogc* derivatives into *B. cenocepacia* K56-2 WT and
881 Δ*ogc* reveals differences in recovery rates of p*ogc*Δ*ogc*X and p*ogc*Δ*ogc*A within
882 *B. cenocepacia* Δ*ogc* (n=4).
883

884

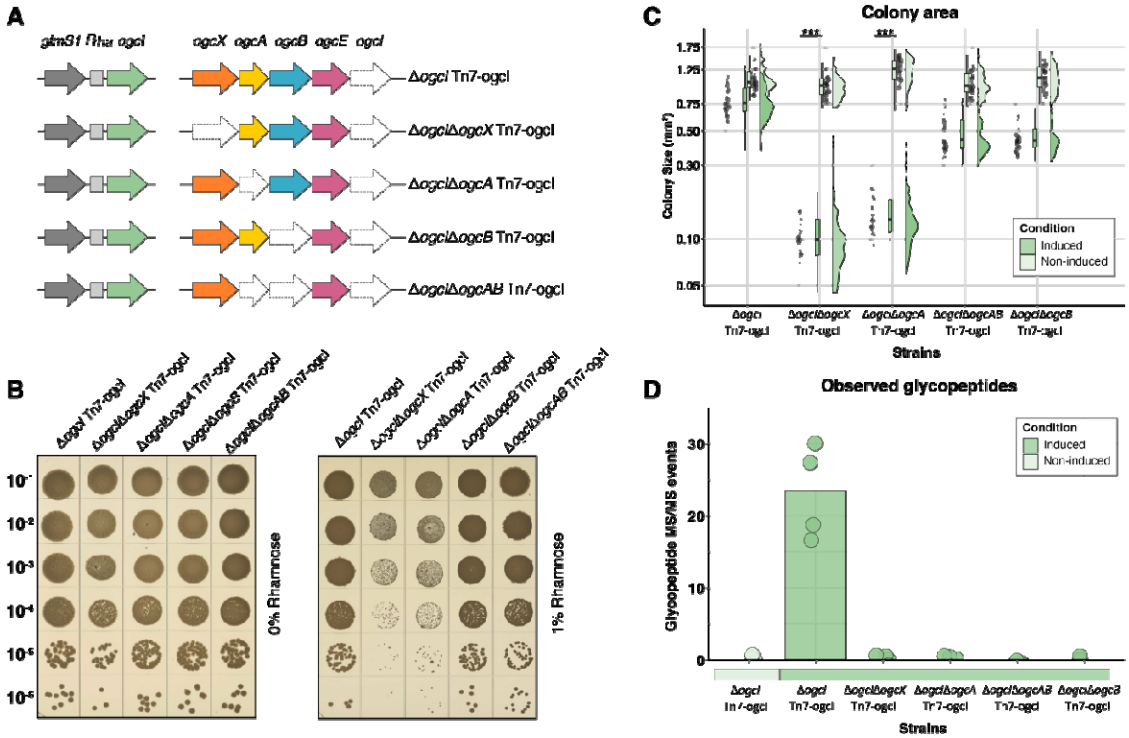

885

886 **Figure 2. Loss of *ogcX* or *ogcA* leads to reduced growth when glycosylation is initiated. A)**
887 Graphic representation of strains Δ*ogcX*, Δ*ogcA*, Δ*ogcB and* Δ*ogcAB* generated within the
888 chromosomal inducible background *B. cenocepacia* Δ*ogcI* Tn7-*ogcI*. **B-C)** Spot plate assays
889 and half-violin box plots assessing growth of strains with and without 1% rhamnose
890 induction. Induction results in reduced colony size of Δ*ogcX* and Δ*ogcA* strains to 10% of the
891 size observed in *B. cenocepacia* Δ*ogcI* Tn7-*ogcI* and strains without induction (n=4). **D)**
892 Quantification of glycopeptides identified from whole-cell proteomic analysis of strains.
893 Glycopeptides were assessed in the absence (light green) or presence (dark green) of
894 rhamnose induction (n=4). Induction of *ogcI* expression by 1% rhamnose led to the
895 restoration of glycosylation only in *B. cenocepacia* Δ*ogcI* Tn7-*ogcI* in contrast, no
896 glycosylation was observed in the Δ*ogcX*, Δ*ogcB*, and Δ*ogcAB* strains.

897

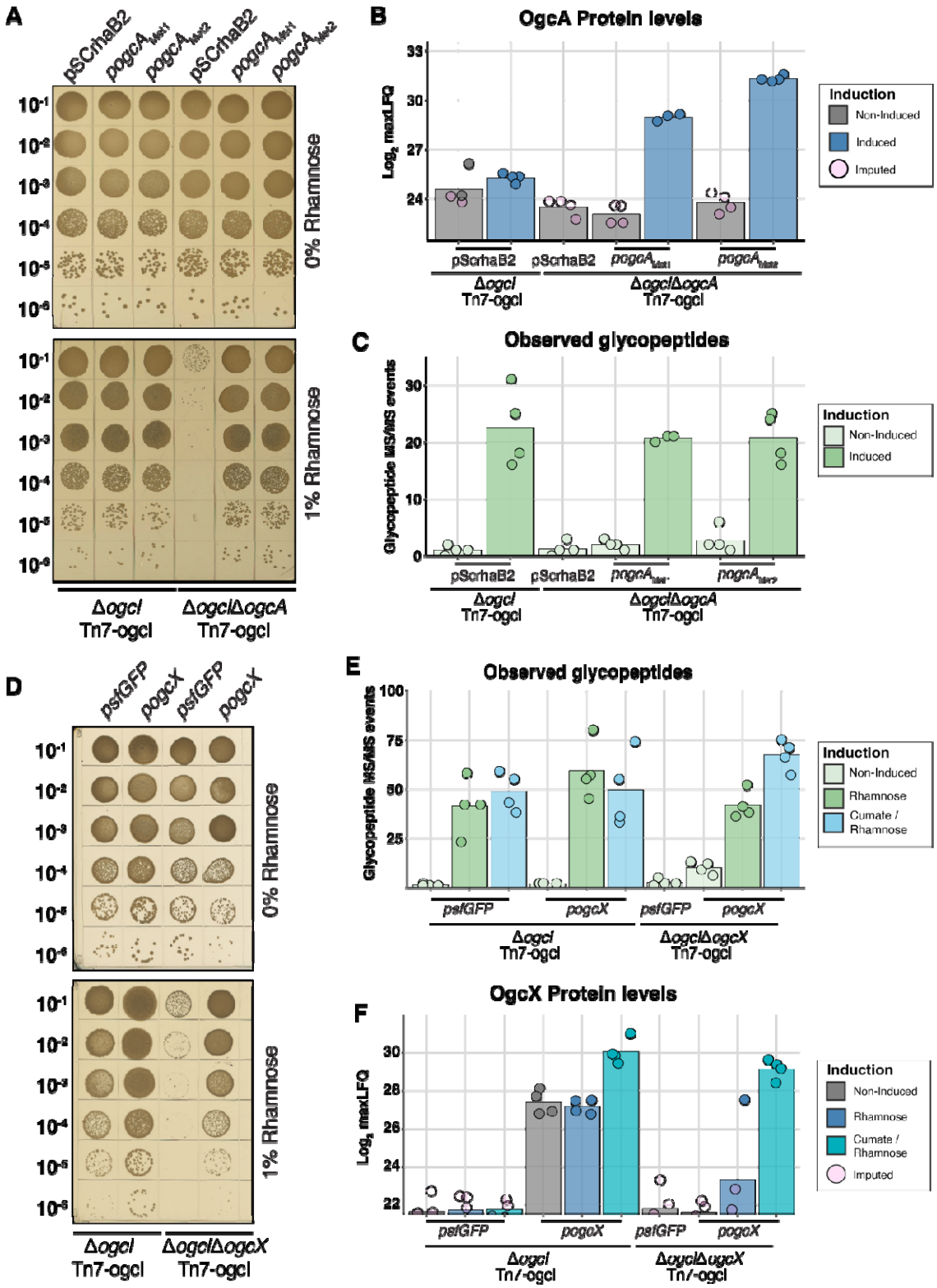

Figure 3. Complementation of Δ*ogcA* and Δ*ogcX* restores growth and glycosylation. A) Spot plate assays of *B. cenocepacia* Δ*ogcI* Tn7-*ogcI* and *B. cenocepacia* Δ*ogcI*Δ*ogcA* Tn7-*ogcI* containing pSCrhaB2 (EV), pSCrhaB2-*ogcA*-Met1 (*ogcA*-Met1), or pSCrhaB2-*ogcA*-Met2

902 (*ogcA*-Met2) with and without 1% rhamnose induction revealing complementation of Δ*ogcA*
903 with *ogcA* variants restores viability and colony size. **B-C)** Quantification of glycopeptides
904 and OgcA levels from whole-cell proteomic analysis of *B. cenocepacia* Δ*ogcI* Tn7-*ogcI* and
905 *B. cenocepacia* Δ*ogcI*Δ*ogcA* Tn7-*ogcI* strains carrying EV, $ogcA_{Met1}$, or $ogcA_{Met2}$. Induction
906 with 1% rhamnose results in the detection of OgcA within *B. cenocepacia* Δ*ogcI*Δ*ogcA* Tn7-
907 *ogcI* and the restoration of glycosylation (n=4, Δ*ogcI* Δ*ogcA* Tn7-*ogcI* *ogcA*-Met1 induced
908 group n=3). **D)** Spot plate assays of *B. cenocepacia* Δ*ogcI* Tn7-*ogcI* and *B. cenocepacia*
909 Δ*ogcI*Δ*ogcX* Tn7-*ogcI* carrying pcumate-sfGFP (sfGFP) and pcumate-*ogcX-his* (p*ogc*X) with
910 and without 1% rhamnose induction revealing complemented Δ*ogcX* restores viability and
911 colony size. **E-F)** Quantification of glycopeptides and OgcX levels from whole-cell proteomic
912 analysis of *B. cenocepacia* Δ*ogcI* Tn7-*ogcI* and *B. cenocepacia* Δ*ogcI*Δ*ogcX* Tn7-*ogcI* strains
913 carrying sfGFP or *ogcX* plasmids. Induction results in the detection of OgcX within
914 *B. cenocepacia* Δ*ogcI*Δ*ogcX* Tn7-*ogcI* and the restoration of glycosylation (n=4).

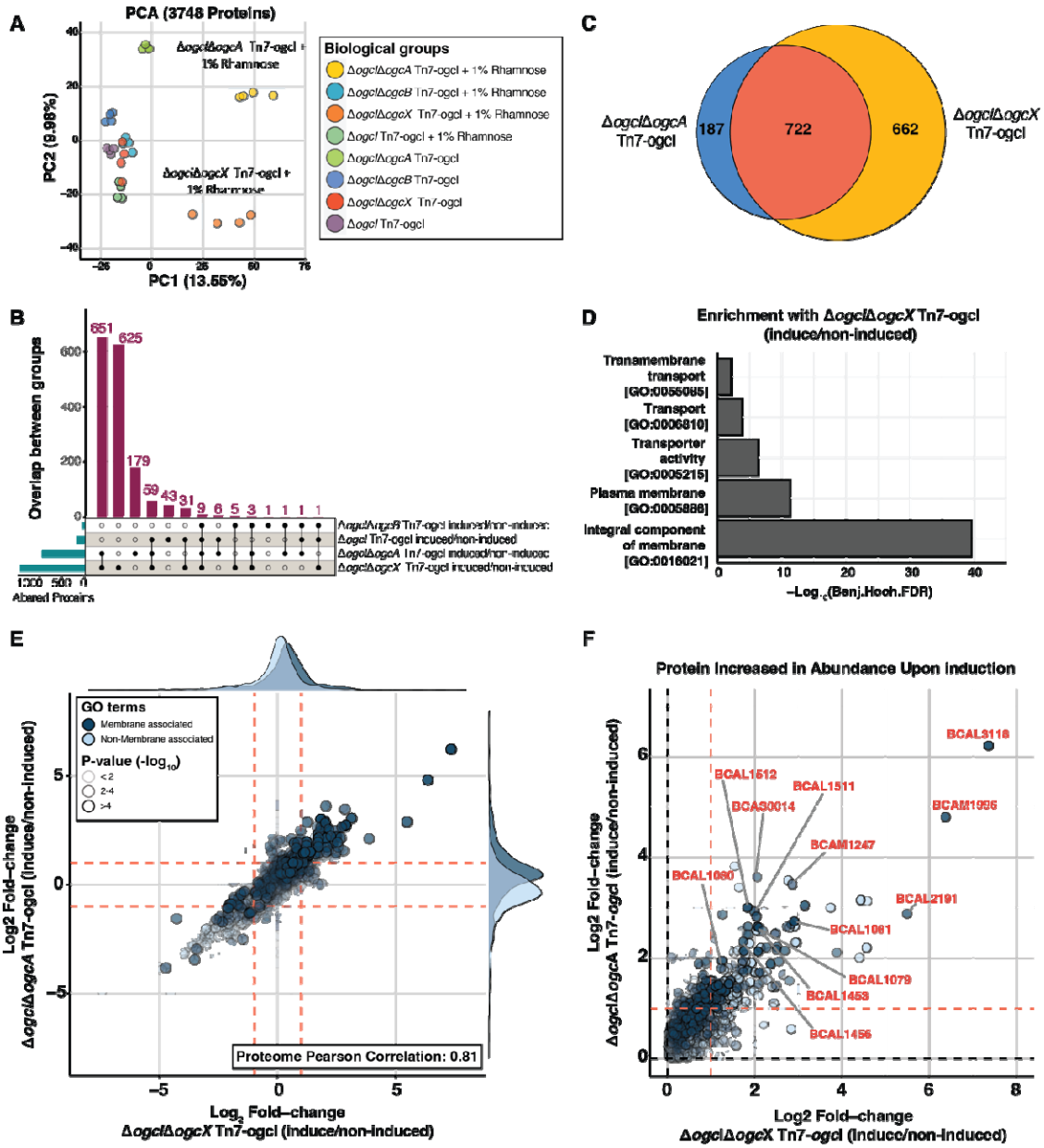

Figure 4. Proteomic analysis of strains in response to glycosylation initiation. DIA proteomic analysis of Δ*ogcl* Tn7-ogcl, Δ*ogcl*Δ*ogcA* Tn7-*ogcl*, Δ*ogcl*Δ*ogcB* Tn7-*ogcl*, and Δ*ogcl*Δ*ogcX* Tn7-*ogcl* strains with and without rhamnose induction (n=4). **A)** Principal component analysis (PCA) of Δ*ogcl* Tn7-*ogcl* strains under induced and non-induced conditions. Biological groups are observed to form distinct clusters, with Δ*ogcl*Δ*ogcA* Tn7-*ogcl* and Δ*ogcl*Δ*ogcX* Tn7-*ogcl* strains separating along PC1 upon induction. **B-C)** Upset plot and Venn diagram of proteomic alterations, defined as >2-fold-change and -$\log_{10}$(p-value) > 2 observed across strains, reveal that induction results in hundreds of protein alterations

within Δ*ogcI*Δ*ogcA* Tn7-*ogcI* and Δ*ogcI*Δ*ogcX* Tn7-*ogcI* strains compared to Δ*ogcI*Δ*ogcB* Tn7-*ogcI* or Δ*ogcI* Tn7-ogcI. **D)** Enrichment analysis of GO terms associated with the altered proteins in Δ*ogcI*Δ*ogcX* Tn7-*ogcI* strain reveals an over-representation of proteomic changes in membrane-associated protein classes. **E)** 2D scatter plots comparing proteome changes observed within Δ*ogcI*Δ*ogcA* Tn7-*ogcI* and Δ*ogcI*Δ*ogcX* Tn7-*ogcI* in response to glycosylation initiation. Proteins associated with membrane GO-terms are color-coded dark blue with the opacity corresponding to the average p-values observed across both comparisons. **F)** Zoomed in 2D scatter plots of proteins observed to increase upon induction within Δ*ogcI*Δ*ogcA* Tn7-*ogcI* and Δ*ogcI*Δ*ogcX* Tn7-*ogcI* with membrane proteins of note highlighted.

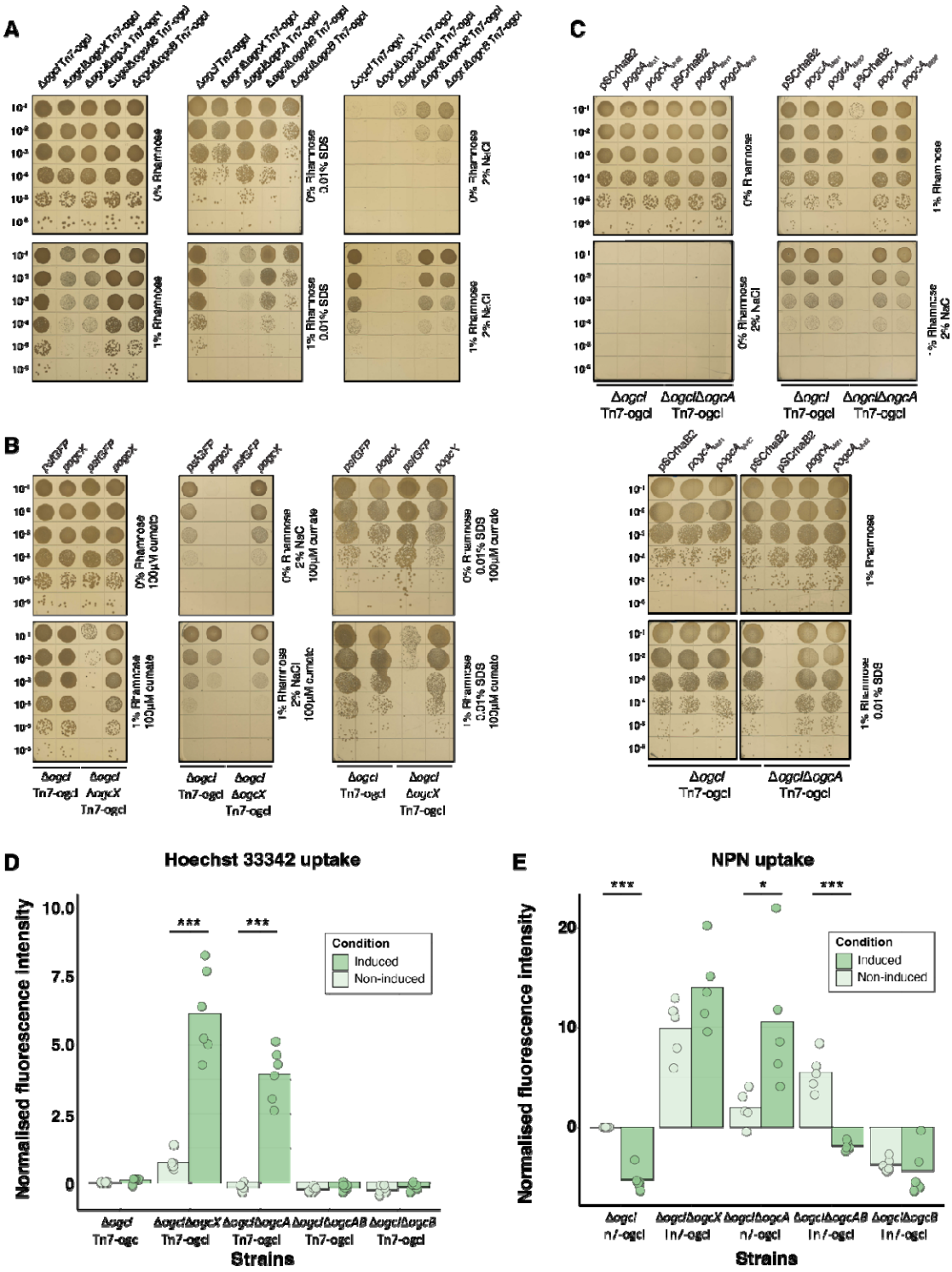

935

936 **Figure 5. Loss of *ogcA* and *ogcX* impacts the membrane integrity of *B. cenocepacia*. A)** Spot
937 plate assays of strains in response to membrane (0.01% SDS) and osmotic (2% NaCl) stress
938 with and without 1% rhamnose induction (n=4). The deletion of ogcX and *ogcA* increases
939 sensitivity to 0.01% SDS when glycosylation is initiated, while both mutants appear sensitive

to osmotic stress (2% NaCl) regardless of induction. **B-C)** Spot plate assays of complemented Δ*ogc*IΔ*ogc*A Tn7-*ogc*I and Δ*ogc*IΔ*ogc*X Tn7-*ogc*I strains in response to membrane (0.01% SDS) and osmotic (2% NaCl) stress with and without 1% rhamnose induction demonstrating the restoration of growth within complemented strains (n=4). **D-E)** Hoechst 33342 and NPN uptake assays of strains reveal loss of *ogcA* and *ogcX* leads to increased fluorescence upon induction, supporting enhanced membrane permeability (n=6 for Hoechst 33342, n=5 for NPN). The fluorescence intensities have been normalised against bacterial viability counts (**Supplementary Figure 11**).

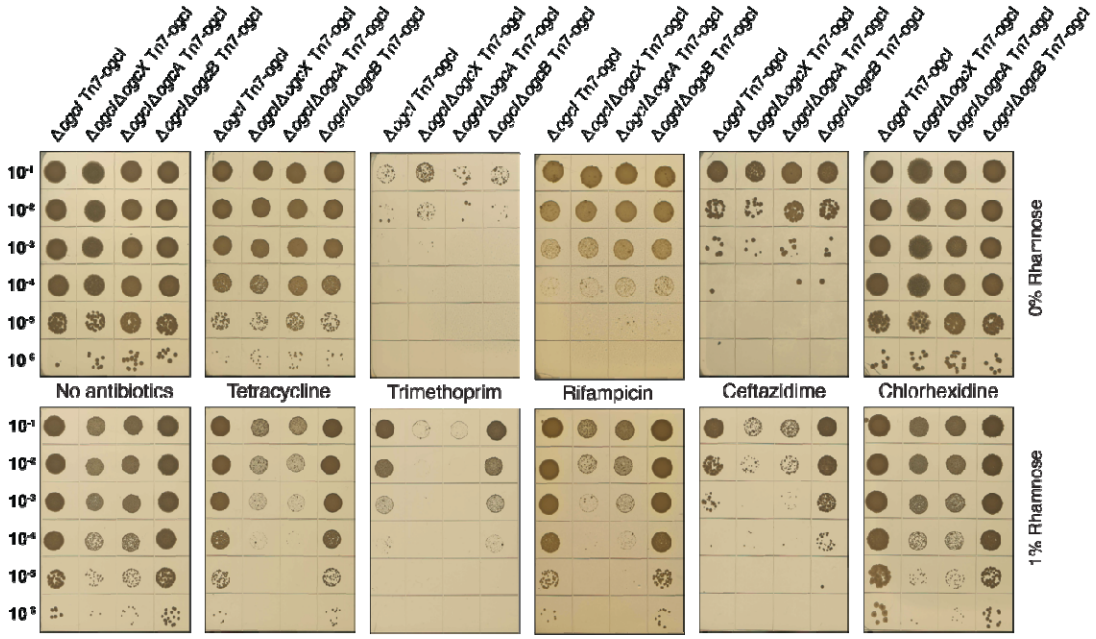

Figure 6. Loss of *ogcA* and *ogcX* sensitises *B. cenocepacia* to antimicrobials. Spot plate assays of *B. cenocepacia* strains, including Δ*ogcI* Tn7-*ogcI*, Δ*ogcI*Δ*ogcX* Tn7-*ogcI*, Δ*ogcI*Δ*ogcA* Tn7-*ogcI*, and Δ*ogcI*Δ*ogcB* Tn7-*ogcI* on CAMHA containing various antibiotics, with or without induction with 1% rhamnose. Rhamnose-induced glycosylation resulted in increased susceptibility to tetracycline, rifampicin, trimethoprim and ceftazidime in strains lacking *ogcA* and *ogcX*. Data representative of four biological replicates per strain per antimicrobial.

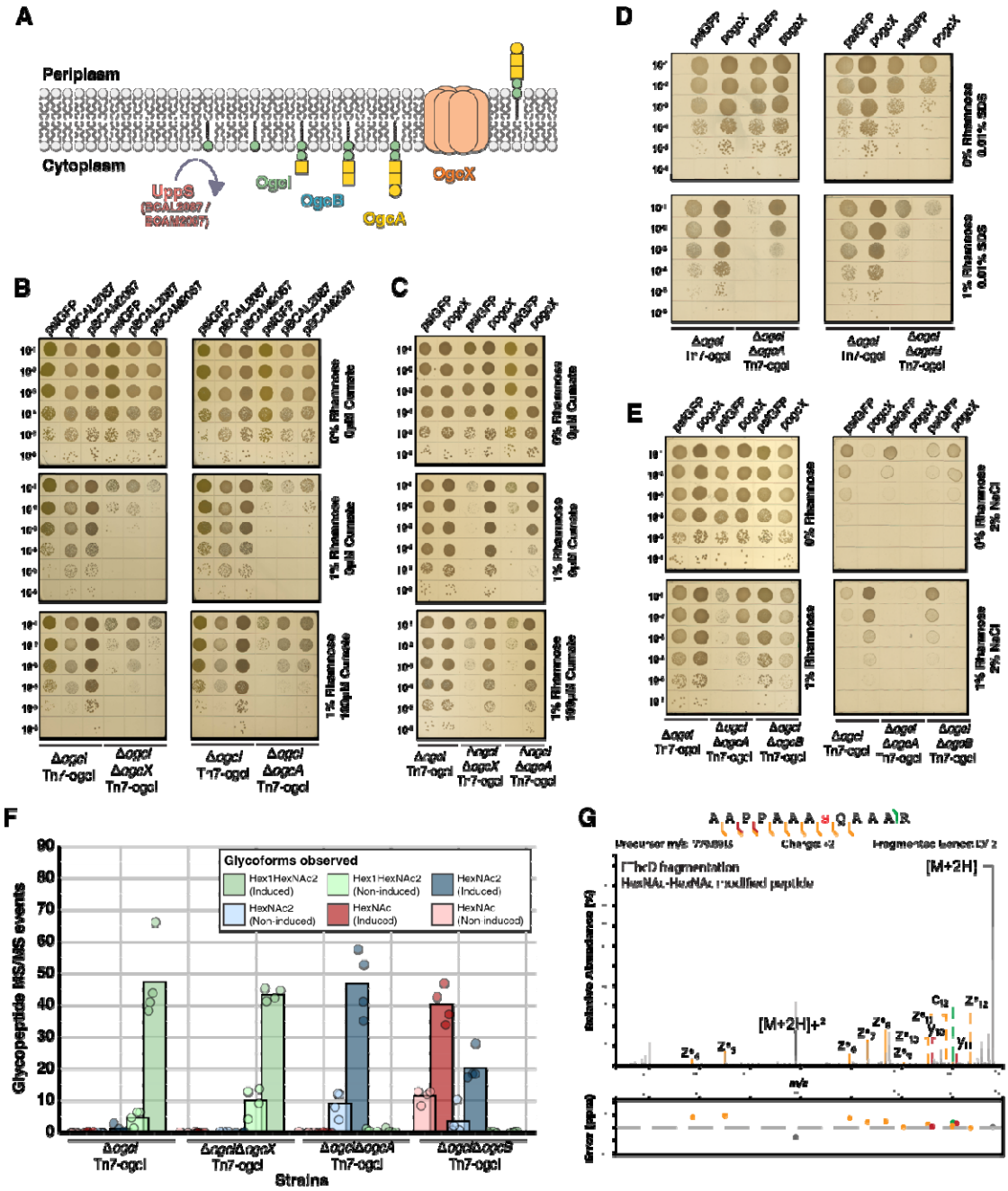

958

959 **Figure 7. Overexpression of UppS or OgcX modulates *ogc* associated defects in**
960 ***B. cenocepacia*. A)** Proposed enzymes responsible for the *de novo* synthesis of the
961 undecaprenyl pool and steps inferred within *ogc* biosynthesis**.** Within *B. cenocepacia*, two
962 putative undecaprenyl pyrophosphate synthases (UppS) are assigned corresponding to
963 BCAL2087 and BCAM2067, while OgcI is responsible for *OGC* initiation and OgcB the
964 addition of the second GalNAc[47]. The functions of OgcA, as the glycotransferase responsible
965 for the addition of the final Gal and OgcX, as the flippase responsible for glycan

966 translocation have only been inferred to date. **B)** Spot plate assays of the *B. cenocepacia*
967 Δ*ogcI* Tn7-*ogcI*, Δ*ogcI*Δ*ogcX* Tn7-*ogcI* and Δ*ogcI*Δ*ogcA* Tn7-*ogcI* containing pcumate-sfGFP,
968 pcumate-BCAL2087 or pcumate-BCAM2067 reveal the initiation of glycosylation reduces
969 viability while induction of putative UppS partially restores the defect observed within
970 Δ*ogcA* and Δ*ogcX* strains (n=4). **C)** Spot plate assays of the *B. cenocepacia* Δ*ogcI* Tn7-*ogcI*,
971 Δ*ogcI*Δ*ogcX* Tn7-*ogcI* and Δ*ogcI*Δ*ogcA* Tn7-*ogcI* containing pcumate-sfGFP (*psfGFP*) and
972 pcumate-ogcX (*pogcX*) demonstrating the complementation of Δ*ogcI*Δ*ogcA* Tn7-*ogcI* with
973 *pogcX* restores growth (n=4). **D and E)** Spot plate assays of the *B. cenocepacia* Δ*ogcI* Tn7-
974 *ogcI*, Δ*ogcI*Δ*ogcA* Tn7-*ogcI* and Δ*ogcI*Δ*ogcB* Tn7-*ogcI* containing pcumate-sfGFP (*psfGFP*)
975 and pcumate-ogcX (*pogcX*) in response to membrane (0.01% SDS) and osmotic (2% NaCl)
976 stresses with glycosylation initiation demonstrating that p*ogcX* restores resistant to stress in
977 Δ*ogcI*Δ*ogcA* Tn7-*ogcI* yet does not suppress the defect observed in Δ*ogcI*Δ*ogcB* Tn7-*ogcI*
978 (n=4). **F)** Quantification of glycopeptides from whole-cell proteomic analysis of
979 *B. cenocepacia* Tn7-*ogcI* strains carrying p*ogcX*. Induction results in the detection of
980 glycosylation within strains with varying glycoforms observed across strains (n=4). **G)** EThcD
981 fragmentation of the HexNAc2 modified peptide ^{397}AAPPAAASQAAAR^{409} (BCAL1674 Uniprot:
982 B4E8U6) confirming the localization of the $HexNAc_2$ glycosylation event residue S^{404}.
983

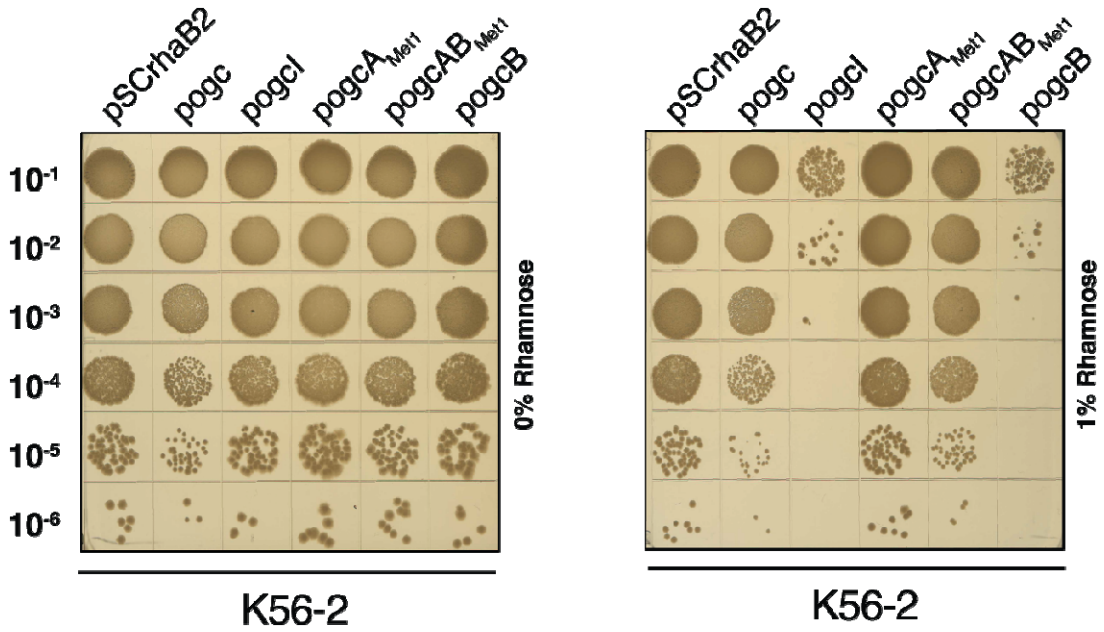

984

985 **Figure 8. Modulation of early steps in *ogc* biosynthesis impacts *B. cenocepacia* viability.**
986 Spot plate assays of *B. cenocepacia* K56-2 (WT) containing the expression vectors pSCrhaB2,
987 pSCrhaB2-*ogc* (p*ogc*), pSCrhaB2-*ogcI* (p*ogcI*), pSCrhaB2-*ogcA-Met1* (p*ogcA*$_{Met1}$), pSCrhaB2-
988 *ogcB* (p*ogcB*), pSCrhaB2-*ogcAB-Met1* (p*ogcAB*$_{Met1}$). Induction of *ogc*I and *ogc*B results in
989 reduced viability, while the expression of *ogc*A and *ogcAB* demonstrated no reduction in
990 viability (n=4).

References:

1 Touz, E. T. & Mengin-Lecreulx, D. Undecaprenyl Phosphate Synthesis. *EcoSal Plus* **3** (2008). https://doi.org:10.1128/ecosalplus.4.7.1.7

2 Workman, S. D. & Strynadka, N. C. J. A Slippery Scaffold: Synthesis and Recycling of the Bacterial Cell Wall Carrier Lipid. *J Mol Biol* **432**, 4964-4982 (2020). https://doi.org:10.1016/j.jmb.2020.03.025

3 Hong, Y., Cunneen, M. M. & Reeves, P. R. The Wzx translocases for Salmonella enterica O-antigen processing have unexpected serotype specificity. *Molecular microbiology* **84**, 620-630 (2012). https://doi.org:10.1111/j.1365-2958.2012.08048.x

4 Liu, M. A., Stent, T. L., Hong, Y. & Reeves, P. R. Inefficient translocation of a truncated O unit by a Salmonella Wzx affects both O-antigen production and cell growth. *FEMS Microbiol Lett* **362** (2015). https://doi.org:10.1093/femsle/fnv053

5 Barreteau, H. *et al.* Quantitative high-performance liquid chromatography analysis of the pool levels of undecaprenyl phosphate and its derivatives in bacterial membranes. *J Chromatogr B Analyt Technol Biomed Life Sci* **877**, 213-220 (2009). https://doi.org:10.1016/j.jchromb.2008.12.010

6 Jorgenson, M. A. & Young, K. D. Interrupting biosynthesis of O-antigen or the lipopolysaccharide core produces morphological defects in Escherichia coli by sequestering undecaprenyl phosphate. *Journal of bacteriology* (2016). https://doi.org:10.1128/JB.00550-16

7 Jorgenson, M. A., Kannan, S., Laubacher, M. E. & Young, K. D. Dead-end intermediates in the enterobacterial common antigen pathway induce morphological defects in Escherichia coli by competing for undecaprenyl phosphate. *Molecular microbiology* **100**, 1-14 (2016). https://doi.org:10.1111/mmi.13284

8 Tatar, L. D., Marolda, C. L., Polischuk, A. N., van Leeuwen, D. & Valvano, M. A. An Escherichia coli undecaprenyl-pyrophosphate phosphatase implicated in undecaprenyl phosphate recycling. *Microbiology (Reading)* **153**, 2518-2529 (2007). https://doi.org:10.1099/mic.0.2007/006312-0

9 Yuasa, R., Levinthal, M. & Nikaido, H. Biosynthesis of cell wall lipopolysaccharide in mutants of Salmonella. V. A mutant of Salmonella typhimurium defective in the synthesis of cytidine diphosphoabequose. *Journal of bacteriology* **100**, 433-444 (1969). https://doi.org:10.1128/jb.100.1.433-444.1969

10 Rick, P. D. *et al.* Evidence that the wzxE gene of Escherichia coli K-12 encodes a protein involved in the transbilayer movement of a trisaccharide-lipid intermediate in the assembly of enterobacterial common antigen. *The Journal of biological chemistry* **278**, 16534-16542 (2003). https://doi.org:10.1074/jbc.M301750200

11 Qin, J., Hong, Y. & Totsika, M. Determining glycosyltransferase functional order via lethality due to accumulated O-antigen intermediates, exemplified with Shigella flexneri O-antigen biosynthesis. *Applied and environmental microbiology* **90**, e0220323 (2024). https://doi.org:10.1128/aem.02203-23

12 Swoboda, J. G. *et al.* Discovery of a small molecule that blocks wall teichoic acid biosynthesis in Staphylococcus aureus. *ACS Chem Biol* **4**, 875-883 (2009). https://doi.org:10.1021/cb900151k

13 Muscato, J. D. *et al.* Rapid Inhibitor Discovery by Exploiting Synthetic Lethality. *J Am Chem Soc* **144**, 3696-3705 (2022). https://doi.org:10.1021/jacs.1c12697

14 Sham, L. T., Zheng, S., Yakhnina, A. A., Kruse, A. C. & Bernhardt, T. G. Loss of specificity variants of WzxC suggest that substrate recognition is coupled with transporter opening in MOP-family flippases. *Molecular microbiology* **109**, 633-641 (2018). https://doi.org:10.1111/mmi.14002

15 Chua, W. Z. *et al*. High-Throughput Mutagenesis and Cross-Complementation Experiments Reveal Substrate Preference and Critical Residues of the Capsule Transporters in Streptococcus pneumoniae. *mBio* **12**, e0261521 (2021). https://doi.org:10.1128/mBio.02615-21

16 Su, T. *et al*. Rewiring the pneumococcal capsule pathway for investigating glycosyltransferase specificity and genetic glycoengineering. *Sci Adv* **9**, eadi8157 (2023). https://doi.org:10.1126/sciadv.adi8157

17 Ruiz, N. Lipid Flippases for Bacterial Peptidoglycan Biosynthesis. *Lipid Insights* **8**, 21-31 (2015). https://doi.org:10.4137/LPI.S31783

18 Cuthbertson, L., Kos, V. & Whitfield, C. ABC transporters involved in export of cell surface glycoconjugates. *Microbiol Mol Biol Rev* **74**, 341-362 (2010). https://doi.org:10.1128/MMBR.00009-10

19 Kuk, A. C. Y., Hao, A. & Lee, S. Y. Structure and Mechanism of the Lipid Flippase MurJ. *Annu Rev Biochem* **91**, 705-729 (2022). https://doi.org:10.1146/annurev-biochem-040320-105145

20 Hong, Y., Liu, M. A. & Reeves, P. R. Progress in Our Understanding of Wzx Flippase for Translocation of Bacterial Membrane Lipid-Linked Oligosaccharide. *Journal of bacteriology* **200** (2018). https://doi.org:10.1128/JB.00154-17

21 Liu, D., Cole, R. A. & Reeves, P. R. An O-antigen processing function for Wzx (RfbX): a promising candidate for O-unit flippase. *Journal of bacteriology* **178**, 2102-2107 (1996). https://doi.org:10.1128/jb.178.7.2102-2107.1996

22 Kenyon, J. J. & Hall, R. M. Variation in the complex carbohydrate biosynthesis loci of Acinetobacter baumannii genomes. *PloS one* **8**, e62160 (2013). https://doi.org:10.1371/journal.pone.0062160

23 Paton, J. C. & Trappetti, C. Streptococcus pneumoniae Capsular Polysaccharide. *Microbiol Spectr* **7** (2019). https://doi.org:10.1128/microbiolspec.GPP3-0019-2018

24 Becker, A. Challenges and perspectives in combinatorial assembly of novel exopolysaccharide biosynthesis pathways. *Front Microbiol* **6**, 687 (2015). https://doi.org:10.3389/fmicb.2015.00687

25 Feldman, M. F. *et al.* The activity of a putative polyisoprenol-linked sugar translocase (Wzx) involved in Escherichia coli O antigen assembly is independent of the chemical structure of the O repeat. *The Journal of biological chemistry* **274**, 35129-35138 (1999).

26 Marolda, C. L., Vicarioli, J. & Valvano, M. A. Wzx proteins involved in biosynthesis of O antigen function in association with the first sugar of the O-specific lipopolysaccharide subunit. *Microbiology (Reading)* **150**, 4095-4105 (2004). https://doi.org:10.1099/mic.0.27456-0

27 Hong, Y. & Reeves, P. R. Diversity of o-antigen repeat unit structures can account for the substantial sequence variation of wzx translocases. *Journal of bacteriology* **196**, 1713-1722 (2014). https://doi.org:10.1128/JB.01323-13

28 Liu, M. A., Morris, P. & Reeves, P. R. Wzx flippases exhibiting complex O-unit preferences require a new model for Wzx-substrate interactions. *Microbiologyopen* **8**, e00655 (2019). https://doi.org:10.1002/mbo3.655

29 Liu, D. & Reeves, P. R. Escherichia coli K12 regains its O antigen. *Microbiology (Reading)* **140 (Pt 1)**, 49-57 (1994). https://doi.org:10.1099/13500872-140-1-49

30 Stevenson, G. *et al.* Structure of the O antigen of Escherichia coli K-12 and the sequence of its rfb gene cluster. *Journal of bacteriology* **176**, 4144-4156 (1994). https://doi.org:10.1128/jb.176.13.4144-4156.1994

31 Barr, K. & Rick, P. D. Biosynthesis of enterobacterial common antigen in Escherichia coli. In vitro synthesis of lipid-linked intermediates. *The Journal of biological chemistry* **262**, 7142-7150 (1987).

32 Barr, K., Ward, S., Meier-Dieter, U., Mayer, H. & Rick, P. D. Characterization of an Escherichia coli rff mutant defective in transfer of N-acetylmannosaminuronic acid (ManNAcA) from UDP-ManNAcA to a lipid-linked intermediate involved in enterobacterial common antigen synthesis. *Journal of bacteriology* **170**, 228-233 (1988). https://doi.org:10.1128/jb.170.1.228-233.1988

33 Burrows, L. L. & Lam, J. S. Effect of wzx (rfbX) mutations on A-band and B-band lipopolysaccharide biosynthesis in Pseudomonas aeruginosa O5. *Journal of bacteriology* **181**, 973-980 (1999). https://doi.org:10.1128/JB.181.3.973-980.1999

34 Xayarath, B. & Yother, J. Mutations blocking side chain assembly, polymerization, or transport of a Wzy-dependent Streptococcus pneumoniae capsule are lethal in the absence of suppressor mutations and can affect polymer transfer to the cell wall. *Journal of bacteriology* **189**, 3369-3381 (2007). https://doi.org:10.1128/JB.01938-06

35 Bai, J. *et al.* Essential Gene Analysis in Acinetobacter baumannii by High-Density Transposon Mutagenesis and CRISPR Interference. *Journal of bacteriology* **203**, e0056520 (2021). https://doi.org:10.1128/JB.00565-20

36 Koomey, M. O-linked protein glycosylation in bacteria: snapshots and current perspectives. *Curr Opin Struct Biol* **56**, 198-203 (2019). https://doi.org:10.1016/j.sbi.2019.03.020

37 Nothaft, H. & Szymanski, C. M. Protein glycosylation in bacteria: sweeter than ever. *Nature reviews. Microbiology* **8**, 765-778 (2010). https://doi.org:10.1038/nrmicro2383

38 Nothaft, H. *et al.* Diversity in the protein N-glycosylation pathways within the Campylobacter genus. *Molecular & cellular proteomics : MCP* **11**, 1203-1219 (2012). https://doi.org:10.1074/mcp.M112.021519

39 Jervis, A. J. *et al.* Characterization of the structurally diverse N-linked glycans of Campylobacter species. *Journal of bacteriology* **194**, 2355-2362 (2012). https://doi.org:10.1128/JB.00042-12

40 Hadjineophytou, C. *et al.* Genetic determinants of genus-Level glycan diversity in a bacterial protein glycosylation system. *PLoS Genet* **15**, e1008532 (2019). https://doi.org:10.1371/journal.pgen.1008532

41 Anonsen, J. H. *et al.* Characterization of a Unique Tetrasaccharide and Distinct Glycoproteome in the O-Linked Protein Glycosylation System of Neisseria elongata subsp. glycolytica. *Journal of bacteriology* **198**, 256-267 (2016). https://doi.org:10.1128/JB.00620-15

42 Vik, A. *et al.* Broad spectrum O-linked protein glycosylation in the human pathogen Neisseria gonorrhoeae. *Proceedings of the National Academy of Sciences of the United States of America* **106**, 4447-4452 (2009). https://doi.org:10.1073/pnas.0809504106

43 Borud, B. *et al.* Genetic, structural, and antigenic analyses of glycan diversity in the O-linked protein glycosylation systems of human Neisseria species. *Journal of bacteriology* **192**, 2816-2829 (2010). https://doi.org:10.1128/JB.00101-10

44 Hadjineophytou, C. *et al.* Sculpting the Bacterial O-Glycoproteome: Functional Analyses of Orthologous Oligosaccharyltransferases with Diverse Targeting Specificities. *mBio*, e0379721 (2022). https://doi.org:10.1128/mbio.03797-21

45 Hayes, A. J., Lewis, J. M., Davies, M. R. & Scott, N. E. Burkholderia PglL enzymes are Serine preferring oligosaccharyltransferases which target conserved proteins

across the Burkholderia genus. *Commun Biol* **4**, 1045 (2021). https://doi.org:10.1038/s42003-021-02588-y

46 Ahmad Izaham, A. R. & Scott, N. E. Open Database Searching Enables the Identification and Comparison of Bacterial Glycoproteomes without Defining Glycan Compositions Prior to Searching. *Molecular & cellular proteomics : MCP* **19**, 1561-1574 (2020). https://doi.org:10.1074/mcp.TIR120.002100

47 Fathy Mohamed, Y. *et al.* A general protein O-glycosylation machinery conserved in Burkholderia species improves bacterial fitness and elicits glycan immunogenicity in humans. *The Journal of biological chemistry* **294**, 13248-13268 (2019). https://doi.org:10.1074/jbc.RA119.009671

48 Iwashkiw, J. A., Vozza, N. F., Kinsella, R. L. & Feldman, M. F. Pour some sugar on it: the expanding world of bacterial protein O-linked glycosylation. *Molecular microbiology* **89**, 14-28 (2013). https://doi.org:10.1111/mmi.12265

49 Nothaft, H. & Szymanski, C. M. New discoveries in bacterial N-glycosylation to expand the synthetic biology toolbox. *Curr Opin Chem Biol* **53**, 16-24 (2019). https://doi.org:10.1016/j.cbpa.2019.05.032

50 Borud, B. & Koomey, M. Sweet complexity: O-linked protein glycosylation in pathogenic Neisseria. *Frontiers in cellular and infection microbiology* **14**, 1407863 (2024). https://doi.org:10.3389/fcimb.2024.1407863

51 Linton, D. *et al.* Functional analysis of the Campylobacter jejuni N-linked protein glycosylation pathway. *Molecular microbiology* **55**, 1695-1703 (2005). https://doi.org:10.1111/j.1365-2958.2005.04519.x

52 Perez, C. *et al.* Structure and mechanism of an active lipid-linked oligosaccharide flippase. *Nature* **524**, 433-438 (2015). https://doi.org:10.1038/nature14953

53 Alaimo, C. *et al.* Two distinct but interchangeable mechanisms for flipping of lipid-linked oligosaccharides. *EMBO J* **25**, 967-976 (2006). https://doi.org:10.1038/sj.emboj.7601024

54 Kahler, C. M. *et al.* Polymorphisms in pilin glycosylation Locus of Neisseria meningitidis expressing class II pili. *Infection and immunity* **69**, 3597-3604 (2001). https://doi.org:10.1128/IAI.69.6.3597-3604.2001

55 Power, P. M. *et al.* Genetic characterization of pilin glycosylation in Neisseria meningitidis. *Microbiology* **146 (Pt 4)**, 967-979 (2000). https://doi.org:10.1099/00221287-146-4-967

56 Aas, F. E., Vik, A., Vedde, J., Koomey, M. & Egge-Jacobsen, W. Neisseria gonorrhoeae O-linked pilin glycosylation: functional analyses define both the biosynthetic pathway and glycan structure. *Molecular microbiology* **65**, 607-624 (2007). https://doi.org:10.1111/j.1365-2958.2007.05806.x

57 Johannessen, C., Koomey, M. & Borud, B. Hypomorphic glycosyltransferase alleles and recoding at contingency loci influence glycan microheterogeneity in the protein glycosylation system of Neisseria species. *Journal of bacteriology* **194**, 5034-5043 (2012). https://doi.org:10.1128/JB.00950-12

58 Wang, N. *et al.* Allelic polymorphisms in a glycosyltransferase gene shape glycan repertoire in the O-linked protein glycosylation system of Neisseria. *Glycobiology* **31**, 477-491 (2021). https://doi.org:10.1093/glycob/cwaa073

59 Lithgow, K. V. *et al.* A general protein O-glycosylation system within the Burkholderia cepacia complex is involved in motility and virulence. *Molecular microbiology* **92**, 116-137 (2014). https://doi.org:10.1111/mmi.12540

60 Gislason, A. S., Turner, K., Domaratzki, M. & Cardona, S. T. Comparative analysis of the Burkholderia cenocepacia K56-2 essential genome reveals cell envelope

functions that are uniquely required for survival in species of the genus Burkholderia. *Microb Genom* **3** (2017). https://doi.org:10.1099/mgen.0.000140

61 Hogan, A. M. *et al.* Profiling cell envelope-antibiotic interactions reveals vulnerabilities to beta-lactams in a multidrug-resistant bacterium. *Nat Commun* **14**, 4815 (2023). https://doi.org:10.1038/s41467-023-40494-5

62 Moule, M. G. *et al.* Genome-wide saturation mutagenesis of Burkholderia pseudomallei K96243 predicts essential genes and novel targets for antimicrobial development. *MBio* **5**, e00926-00913 (2014). https://doi.org:10.1128/mBio.00926-13

63 Oppy, C. C. *et al.* Loss of O-linked protein glycosylation in Burkholderia cenocepacia impairs biofilm formation, siderophore activity and alters transcriptional regulators *mSphere* **4**, e00660-00619 (2019).

64 Cardona, S. T. & Valvano, M. A. An expression vector containing a rhamnose-inducible promoter provides tightly regulated gene expression in Burkholderia cenocepacia. *Plasmid* **54**, 219-228 (2005). https://doi.org:10.1016/j.plasmid.2005.03.004

65 Lopez, C. M., Rholl, D. A., Trunck, L. A. & Schweizer, H. P. Versatile dual-technology system for markerless allele replacement in Burkholderia pseudomallei. *Applied and environmental microbiology* **75**, 6496-6503 (2009). https://doi.org:10.1128/AEM.01669-09

66 Aubert, D. F., Hamad, M. A. & Valvano, M. A. A markerless deletion method for genetic manipulation of Burkholderia cenocepacia and other multidrug-resistant gram-negative bacteria. *Methods in molecular biology* **1197**, 311-327 (2014). https://doi.org:10.1007/978-1-4939-1261-2_18

67 Garcia, E. C., Anderson, M. S., Hagar, J. A. & Cotter, P. A. Burkholderia BcpA mediates biofilm formation independently of interbacterial contact-dependent growth inhibition. *Molecular microbiology* **89**, 1213-1225 (2013). https://doi.org:10.1111/mmi.12339

68 Flannagan, R. S., Linn, T. & Valvano, M. A. A system for the construction of targeted unmarked gene deletions in the genus Burkholderia. *Environ Microbiol* **10**, 1652-1660 (2008). https://doi.org:10.1111/j.1462-2920.2008.01576.x

69 Gibson, D. G. *et al.* Enzymatic assembly of DNA molecules up to several hundred kilobases. *Nature methods* **6**, 343-345 (2009). https://doi.org:10.1038/nmeth.1318

70 Lefebre, M. D. & Valvano, M. A. Construction and evaluation of plasmid vectors optimized for constitutive and regulated gene expression in Burkholderia cepacia complex isolates. *Applied and environmental microbiology* **68**, 5956-5964 (2002).

71 Sambrook, J., E. F. Fritsch, and T. Maniatis. *Molecular cloning: a laboratory manual*. (Cold Spring Harbor Laboratory, Cold Spring Harbor, 1990).

72 Figurski, D. H. & Helinski, D. R. Replication of an origin-containing derivative of plasmid RK2 dependent on a plasmid function provided in trans. *Proceedings of the National Academy of Sciences of the United States of America* **76**, 1648-1652 (1979). https://doi.org:10.1073/pnas.76.4.1648

73 Choi, K. H., DeShazer, D. & Schweizer, H. P. mini-Tn7 insertion in bacteria with multiple glmS-linked attTn7 sites: example Burkholderia mallei ATCC 23344. *Nature protocols* **1**, 162-169 (2006). https://doi.org:10.1038/nprot.2006.25

74 Hamad, M. A., Di Lorenzo, F., Molinaro, A. & Valvano, M. A. Aminoarabinose is essential for lipopolysaccharide export and intrinsic antimicrobial peptide resistance in Burkholderia cenocepacia(dagger). *Molecular microbiology* **85**, 962-974 (2012). https://doi.org:10.1111/j.1365-2958.2012.08154.x

75 Bernier, S. P., Son, S. & Surette, M. G. The Mla Pathway Plays an Essential Role in the Intrinsic Resistance of Burkholderia cepacia Complex Species to Antimicrobials

and Host Innate Components. *Journal of bacteriology* **200** (2018). https://doi.org:10.1128/JB.00156-18

76 Malinverni, J. C. & Silhavy, T. J. An ABC transport system that maintains lipid asymmetry in the gram-negative outer membrane. *Proceedings of the National Academy of Sciences of the United States of America* **106**, 8009-8014 (2009). https://doi.org:10.1073/pnas.0903229106

77 Mychack, A. *et al.* A synergistic role for two predicted inner membrane proteins of Escherichia coli in cell envelope integrity. *Molecular microbiology* **111**, 317-337 (2019). https://doi.org:10.1111/mmi.14157

78 Schindelin, J. *et al.* Fiji: an open-source platform for biological-image analysis. *Nature methods* **9**, 676-682 (2012). https://doi.org:10.1038/nmeth.2019

79 Jassem, A. N. *et al.* In vitro susceptibility of Burkholderia vietnamiensis to aminoglycosides. *Antimicrobial agents and chemotherapy* **55**, 2256-2264 (2011). https://doi.org:10.1128/AAC.01434-10

80 Richmond, G. E., Chua, K. L. & Piddock, L. J. Efflux in Acinetobacter baumannii can be determined by measuring accumulation of H33342 (bis-benzamide). *J Antimicrob Chemother* **68**, 1594-1600 (2013). https://doi.org:10.1093/jac/dkt052

81 Krishnamoorthy, G. *et al.* Efflux Pumps of Burkholderia thailandensis Control the Permeability Barrier of the Outer Membrane. *Antimicrobial agents and chemotherapy* **63** (2019). https://doi.org:10.1128/AAC.00956-19

82 Helander, I. M. & Mattila-Sandholm, T. Fluorometric assessment of gram-negative bacterial permeabilization. *J Appl Microbiol* **88**, 213-219 (2000). https://doi.org:10.1046/j.1365-2672.2000.00971.x

83 Loh, B., Grant, C. & Hancock, R. E. Use of the fluorescent probe 1-N-phenylnaphthylamine to study the interactions of aminoglycoside antibiotics with the outer membrane of Pseudomonas aeruginosa. *Antimicrobial agents and chemotherapy* **26**, 546-551 (1984). https://doi.org:10.1128/AAC.26.4.546

84 Malott, R. J., Steen-Kinnaird, B. R., Lee, T. D. & Speert, D. P. Identification of hopanoid biosynthesis genes involved in polymyxin resistance in Burkholderia multivorans. *Antimicrobial agents and chemotherapy* **56**, 464-471 (2012). https://doi.org:10.1128/AAC.00602-11

85 Kulak, N. A., Pichler, G., Paron, I., Nagaraj, N. & Mann, M. Minimal, encapsulated proteomic-sample processing applied to copy-number estimation in eukaryotic cells. *Nature methods* **11**, 319-324 (2014). https://doi.org:10.1038/nmeth.2834

86 Harney, D. J. *et al.* Proteomic Analysis of Human Plasma during Intermittent Fasting. *Journal of proteome research* **18**, 2228-2240 (2019). https://doi.org:10.1021/acs.jproteome.9b00090

87 Rappsilber, J., Mann, M. & Ishihama, Y. Protocol for micro-purification, enrichment, pre-fractionation and storage of peptides for proteomics using StageTips. *Nature protocols* **2**, 1896-1906 (2007). https://doi.org:10.1038/nprot.2007.261

88 Ahmad Izaham, A. R. *et al.* What Are We Missing by Using Hydrophilic Enrichment? Improving Bacterial Glycoproteome Coverage Using Total Proteome and FAIMS Analyses. *Journal of proteome research* **20**, 599-612 (2021). https://doi.org:10.1021/acs.jproteome.0c00565

89 Saba, J., Dutta, S., Hemenway, E. & Viner, R. Increasing the productivity of glycopeptides analysis by using higher-energy collision dissociation-accurate mass-product-dependent electron transfer dissociation. *Int J Proteomics* **2012**, 560391 (2012). https://doi.org:10.1155/2012/560391

90 Caval, T., Zhu, J. & Heck, A. J. R. Simply Extending the Mass Range in Electron Transfer Higher Energy Collisional Dissociation Increases Confidence in N-

Glycopeptide Identification. *Anal Chem* **91**, 10401-10406 (2019). https://doi.org:10.1021/acs.analchem.9b02125

91 Polasky, D. A., Geiszler, D. J., Yu, F. & Nesvizhskii, A. I. Multi-attribute Glycan Identification and FDR Control for Glycoproteomics. *Molecular & cellular proteomics : MCP*, 100205 (2022). https://doi.org:https://doi.org/10.1016/j.mcpro.2022.100205

92 Kong, A. T., Leprevost, F. V., Avtonomov, D. M., Mellacheruvu, D. & Nesvizhskii, A. I. MSFragger: ultrafast and comprehensive peptide identification in mass spectrometry-based proteomics. *Nature methods* **14**, 513-520 (2017). https://doi.org:10.1038/nmeth.4256

93 Polasky, D. A., Yu, F., Teo, G. C. & Nesvizhskii, A. I. Fast and comprehensive N- and O-glycoproteomics analysis with MSFragger-Glyco. *Nature methods* **17**, 1125-1132 (2020). https://doi.org:10.1038/s41592-020-0967-9

94 Holden, M. T. *et al.* The genome of Burkholderia cenocepacia J2315, an epidemic pathogen of cystic fibrosis patients. *Journal of bacteriology* **191**, 261-277 (2009). https://doi.org:10.1128/JB.01230-08

95 Wickham, H. *ggplot2: Elegant Graphics for Data Analysis*. (Springer-Verlag New York, 2016).

96 Brademan, D. R., Riley, N. M., Kwiecien, N. W. & Coon, J. J. Interactive Peptide Spectral Annotator: A Versatile Web-based Tool for Proteomic Applications. *Molecular & cellular proteomics : MCP* **18**, S193-S201 (2019). https://doi.org:10.1074/mcp.TIR118.001209

97 Varga, J. J. *et al.* Draft Genome Sequences of Burkholderia cenocepacia ET12 Lineage Strains K56-2 and BC7. *Genome Announc* **1** (2013). https://doi.org:10.1128/genomeA.00841-13

98 Cox, J. *et al.* Accurate proteome-wide label-free quantification by delayed normalization and maximal peptide ratio extraction, termed MaxLFQ. *Molecular & cellular proteomics : MCP* **13**, 2513-2526 (2014). https://doi.org:10.1074/mcp.M113.031591

99 Tyanova, S. *et al.* The Perseus computational platform for comprehensive analysis of (prote)omics data. *Nature methods* **13**, 731-740 (2016). https://doi.org:10.1038/nmeth.3901

100 Perez-Riverol, Y. *et al.* The PRIDE database and related tools and resources in 2019: improving support for quantification data. *Nucleic Acids Res* **47**, D442-D450 (2019). https://doi.org:10.1093/nar/gky1106

101 Vizcaino, J. A. *et al.* 2016 update of the PRIDE database and its related tools. *Nucleic Acids Res* **44**, D447-456 (2016). https://doi.org:10.1093/nar/gkv1145

102 Ludwig, C. *et al.* Data-independent acquisition-based SWATH-MS for quantitative proteomics: a tutorial. *Mol Syst Biol* **14**, e8126 (2018). https://doi.org:10.15252/msb.20178126

103 Pino, L. K., Just, S. C., MacCoss, M. J. & Searle, B. C. Acquiring and Analyzing Data Independent Acquisition Proteomics Experiments without Spectrum Libraries. *Molecular & cellular proteomics : MCP* **19**, 1088-1103 (2020). https://doi.org:10.1074/mcp.P119.001913

104 Mitchell, A. M., Srikumar, T. & Silhavy, T. J. Cyclic Enterobacterial Common Antigen Maintains the Outer Membrane Permeability Barrier of Escherichia coli in a Manner Controlled by YhdP. *mBio* **9** (2018). https://doi.org:10.1128/mBio.01321-18

105 Jorgenson, M. A. *et al.* Simultaneously inhibiting undecaprenyl phosphate production and peptidoglycan synthases promotes rapid lysis in Escherichia coli. *Molecular microbiology* **112**, 233-248 (2019). https://doi.org:10.1111/mmi.14265

106 D'Elia, M. A. *et al.* Lesions in teichoic acid biosynthesis in Staphylococcus aureus lead to a lethal gain of function in the otherwise dispensable pathway. *Journal of bacteriology* **188**, 4183-4189 (2006). https://doi.org:10.1128/JB.00197-06

107 D'Elia, M. A., Millar, K. E., Beveridge, T. J. & Brown, E. D. Wall teichoic acid polymers are dispensable for cell viability in Bacillus subtilis. *Journal of bacteriology* **188**, 8313-8316 (2006). https://doi.org:10.1128/JB.01336-06

108 Lewis, J. M. & Scott, N. E. CRISPRi-Mediated Silencing of Burkholderia O-Linked Glycosylation Systems Enables the Depletion of Glycosylation Yet Results in Modest Proteome Impacts. *Journal of proteome research* **22**, 1762-1778 (2023). https://doi.org:10.1021/acs.jproteome.2c00790

109 Lewis, J. M., Jebeli, L., Coulon, P. M. L., Lay, C. E. & Scott, N. E. Glycoproteomic and proteomic analysis of Burkholderia cenocepacia reveals glycosylation events within FliF and MotB are dispensable for motility. *Microbiol Spectr* **12**, e0034624 (2024). https://doi.org:10.1128/spectrum.00346-24

110 Tkalec, K. I. *et al.* Glycan-Tailored Glycoproteomic Analysis Reveals Serine is the Sole Residue Subjected to O-Linked Glycosylation in Acinetobacter baumannii. *Journal of proteome research* **23**, 2474-2494 (2024). https://doi.org:10.1021/acs.jproteome.4c00148

111 Scott, N. E. *et al.* Diversity within the O-linked protein glycosylation systems of acinetobacter species. *Molecular & cellular proteomics : MCP* **13**, 2354-2370 (2014). https://doi.org:10.1074/mcp.M114.038315

112 Iwashkiw, J. A. *et al.* Identification of a general O-linked protein glycosylation system in Acinetobacter baumannii and its role in virulence and biofilm formation. *PLoS pathogens* **8**, e1002758 (2012). https://doi.org:10.1371/journal.ppat.1002758

113 Naess, L. M. *et al.* Genetic, Functional, and Immunogenic Analyses of the O-Linked Protein Glycosylation System in Neisseria meningitidis Serogroup A ST-7 Isolates. *Journal of bacteriology* **205**, e0045822 (2023). https://doi.org:10.1128/jb.00458-22

114 Kuhn, H. M., Meier-Dieter, U. & Mayer, H. ECA, the enterobacterial common antigen. *FEMS microbiology reviews* **4**, 195-222 (1988). https://doi.org:10.1111/j.1574-6968.1988.tb02743.x

115 Rai, A. K. & Mitchell, A. M. Enterobacterial Common Antigen: Synthesis and Function of an Enigmatic Molecule. *mBio* **11** (2020). https://doi.org:10.1128/mBio.01914-20

116 Kajimura, J., Rahman, A. & Rick, P. D. Assembly of cyclic enterobacterial common antigen in Escherichia coli K-12. *Journal of bacteriology* **187**, 6917-6927 (2005). https://doi.org:10.1128/JB.187.20.6917-6927.2005

117 Mohamed, Y. F. & Valvano, M. A. A Burkholderia cenocepacia MurJ (MviN) homolog is essential for cell wall peptidoglycan synthesis and bacterial viability. *Glycobiology* **24**, 564-576 (2014). https://doi.org:10.1093/glycob/cwu025

118 Cain, A. K. *et al.* A decade of advances in transposon-insertion sequencing. *Nat Rev Genet* **21**, 526-540 (2020). https://doi.org:10.1038/s41576-020-0244-x

119 Mateus, A. *et al.* Transcriptional and Post-Transcriptional Polar Effects in Bacterial Gene Deletion Libraries. *mSystems* **6**, e0081321 (2021). https://doi.org:10.1128/mSystems.00813-21

120 Hutchison, C. A., 3rd *et al.* Polar Effects of Transposon Insertion into a Minimal Bacterial Genome. *Journal of bacteriology* **201** (2019). https://doi.org:10.1128/JB.00185-19

121 Sass, A., Everaert, A., Van Acker, H., Van den Driessche, F. & Coenye, T. Targeting the Nonmevalonate Pathway in Burkholderia cenocepacia Increases Susceptibility to

Certain beta-Lactam Antibiotics. *Antimicrobial agents and chemotherapy* **62** (2018). https://doi.org:10.1128/AAC.02607-17

122 Zhao, L., Chang, W. C., Xiao, Y., Liu, H. W. & Liu, P. Methylerythritol phosphate pathway of isoprenoid biosynthesis. *Annu Rev Biochem* **82**, 497-530 (2013). https://doi.org:10.1146/annurev-biochem-052010-100934

123 Moya, B. *et al.* Beta-lactam resistance response triggered by inactivation of a nonessential penicillin-binding protein. *PLoS pathogens* **5**, e1000353 (2009). https://doi.org:10.1371/journal.ppat.1000353

124 Zamorano, L. *et al.* The Pseudomonas aeruginosa CreBC two-component system plays a major role in the response to beta-lactams, fitness, biofilm growth, and global regulation. *Antimicrobial agents and chemotherapy* **58**, 5084-5095 (2014). https://doi.org:10.1128/AAC.02556-14

125 Huang, H. H. *et al.* Expression and Functions of CreD, an Inner Membrane Protein in Stenotrophomonas maltophilia. *PloS one* **10**, e0145009 (2015). https://doi.org:10.1371/journal.pone.0145009

126 Reid, C. W., Stupak, J., Szymanski, C. M. & Li, J. Analysis of bacterial lipid-linked oligosaccharide intermediates using porous graphitic carbon liquid chromatography-electrospray ionization mass spectrometry: heterogeneity in the polyisoprenyl carrier revealed. *Anal Chem* **81**, 8472-8478 (2009). https://doi.org:10.1021/ac9013622

127 Horzempa, J., Dean, C. R., Goldberg, J. B. & Castric, P. Pseudomonas aeruginosa 1244 pilin glycosylation: glycan substrate recognition. *Journal of bacteriology* **188**, 4244-4252 (2006). https://doi.org:10.1128/JB.00273-06

128 Castric, P., Cassels, F. J. & Carlson, R. W. Structural characterization of the Pseudomonas aeruginosa 1244 pilin glycan. *The Journal of biological chemistry* **276**, 26479-26485 (2001). https://doi.org:10.1074/jbc.M102685200

129 Lees-Miller, R. G. *et al.* A common pathway for O-linked protein-glycosylation and synthesis of capsule in Acinetobacter baumannii. *Molecular microbiology* **89**, 816-830 (2013). https://doi.org:10.1111/mmi.12300

130 Knoot, C. J. *et al.* Discovery and characterization of a new class of O-linking oligosaccharyltransferases from the Moraxellaceae family. *Glycobiology* (2022). https://doi.org:10.1093/glycob/cwac070

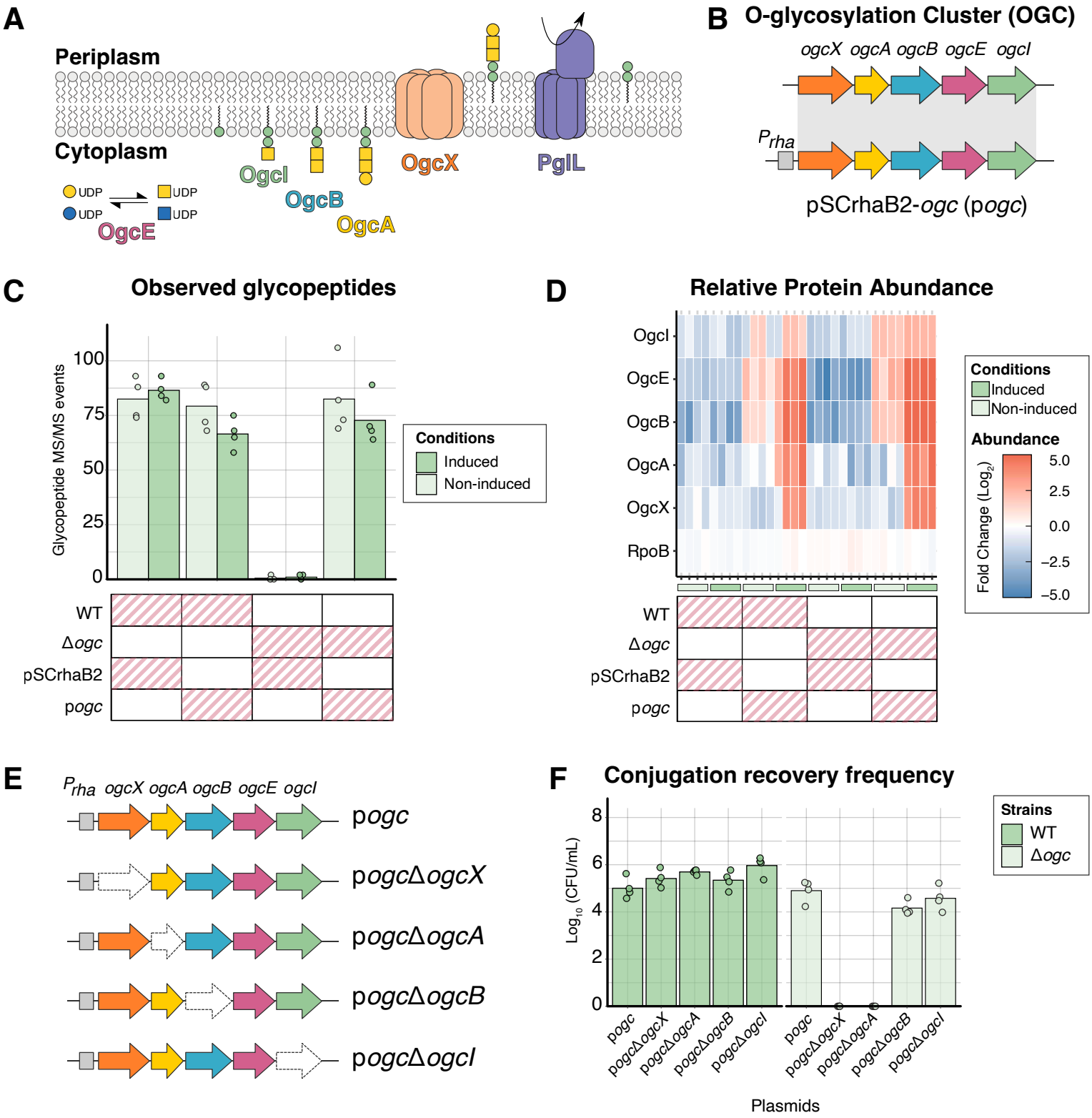
A
Periplasm
Cytoplasm
UDP
UDP
UDP
UDP
OgcE
OgcI
OgcB
OgcA
OgcX
PglL
B
O-glycosylation Cluster (OGC)
ogcX ogcA ogcB ogcE ogcI
Prha
pSCrhaB2-ogc (pogc)
C
Observed glycopeptides
Glycopeptide MS/MS events
100
75
50
25
0
Conditions
Induced
Non-induced
WT
Δogc
pSCrhaB2
pogc
D
Relative Protein Abundance
OgcI
OgcE
OgcB
OgcA
OgcX
RpoB
Conditions
Induced
Non-induced
Abundance
Fold Change (Log2)
5.0
2.5
0.0
−2.5
−5.0
WT
Δogc
pSCrhaB2
pogc
E
Prha ogcX ogcA ogcB ogcE ogcI
pogc
pogcΔogcX
pogcΔogcA
pogcΔogcB
pogcΔogcI
F
Conjugation recovery frequency
Log10 (CFU/mL)
8
6
4
2
0
pogc
pogcΔogcX
pogcΔogcA
pogcΔogcB
pogcΔogcI
pogc
pogcΔogcX
pogcΔogcA
pogcΔogcB
pogcΔogcI
Plasmids
Strains
WT
Δogc

Figure 1

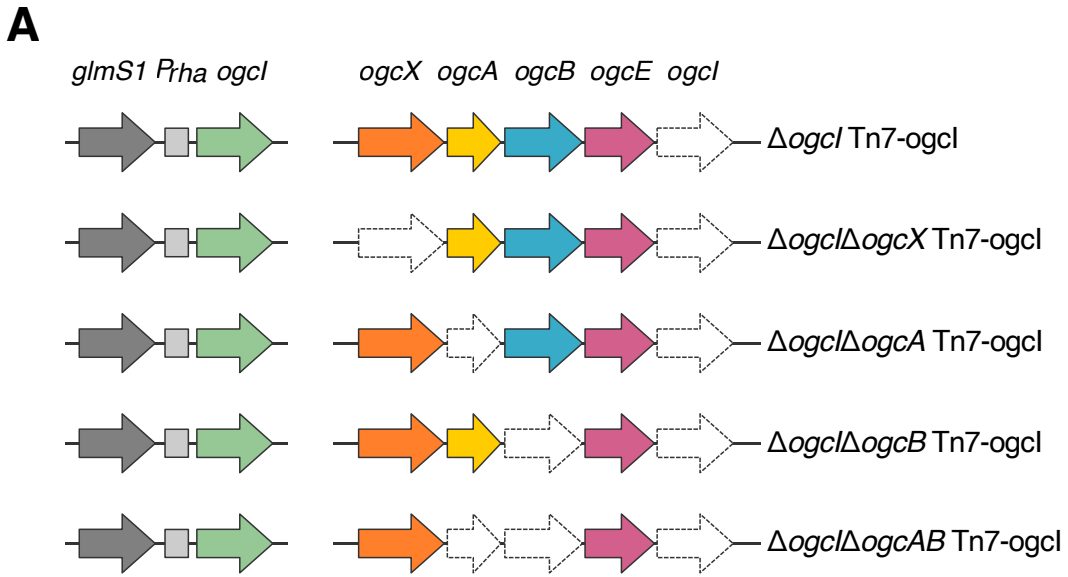
A
glmS1 PRha ogcI
ogcX ogcA ogcB ogcE ogcI
ΔogcI Tn7-ogcI
ΔogcIΔogcX Tn7-ogcI
ΔogcIΔogcA Tn7-ogcI
ΔogcIΔogcB Tn7-ogcI
ΔogcIΔogcAB Tn7-ogcI

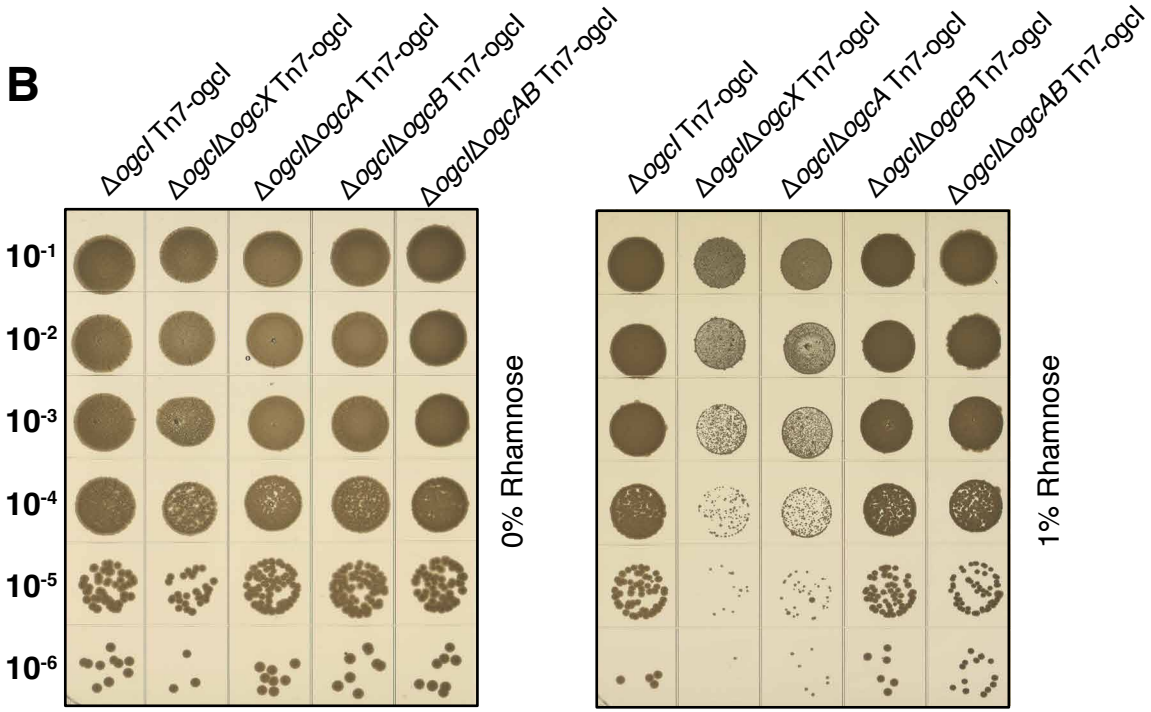
B
ΔogcI Tn7-ogcI
ΔogcIΔogcX Tn7-ogcI
ΔogcIΔogcA Tn7-ogcI
ΔogcIΔogcB Tn7-ogcI
ΔogcIΔogcAB Tn7-ogcI
10-1
10-2
10-3
10-4
10-5
10-6
0% Rhamnose
1% Rhamnose

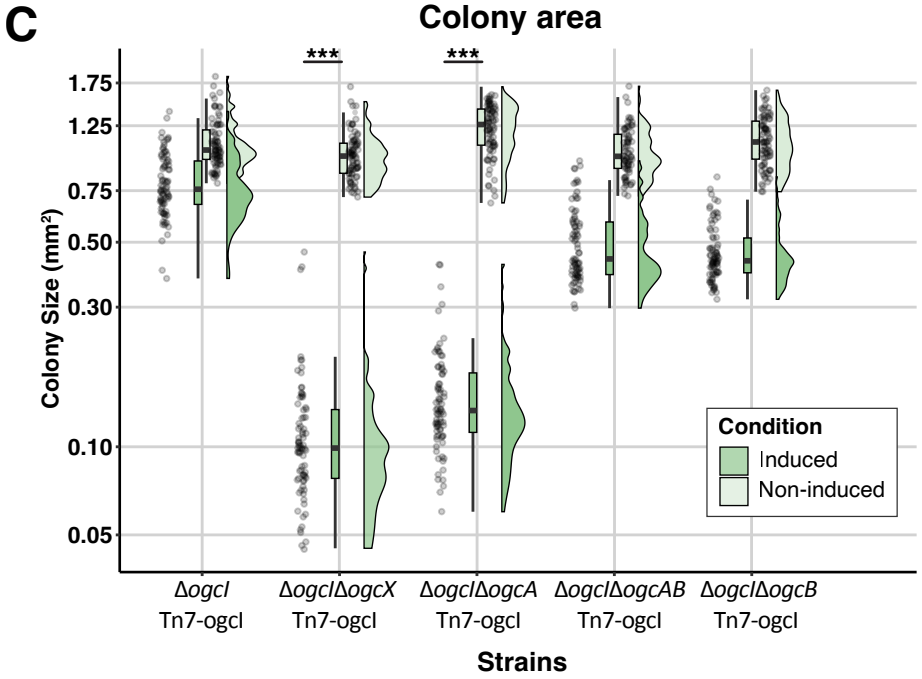
C
Colony area
Colony Size (mm²)
1.75
1.25
0.75
0.50
0.30
0.10
0.05
***
***
Condition
Induced
Non-induced
ΔogcI Tn7-ogcI
ΔogcIΔogcX Tn7-ogcI
ΔogcIΔogcA Tn7-ogcI
ΔogcIΔogcAB Tn7-ogcI
ΔogcIΔogcB Tn7-ogcI
Strains

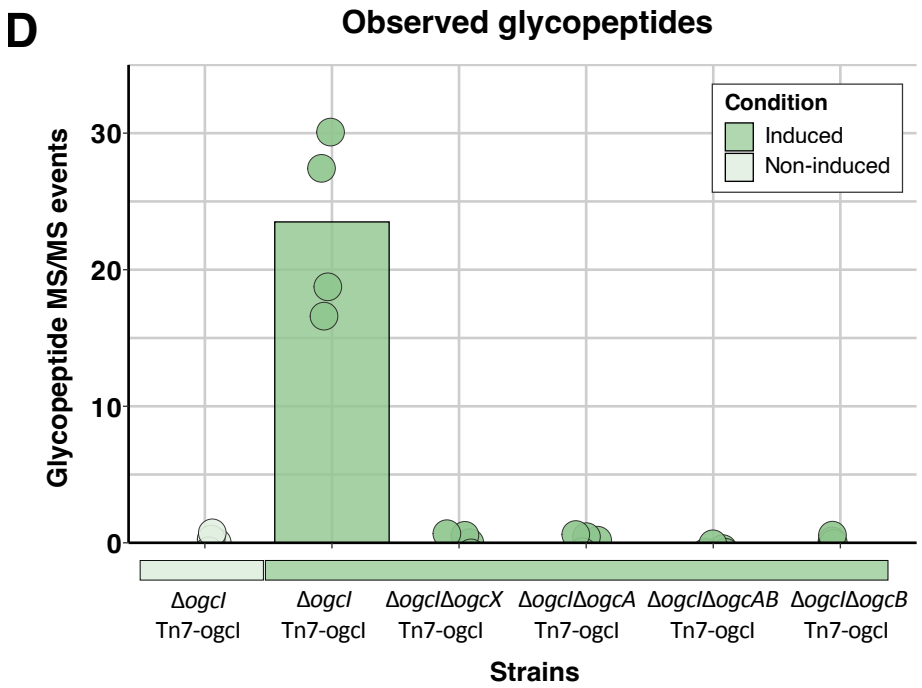
D
Observed glycopeptides
Glycopeptide MS/MS events
30
20
10
0
Condition
Induced
Non-induced
ΔogcI Tn7-ogcI
ΔogcI Tn7-ogcI
ΔogcIΔogcX Tn7-ogcI
ΔogcIΔogcA Tn7-ogcI
ΔogcIΔogcAB Tn7-ogcI
ΔogcIΔogcB Tn7-ogcI
Strains

Figure 2

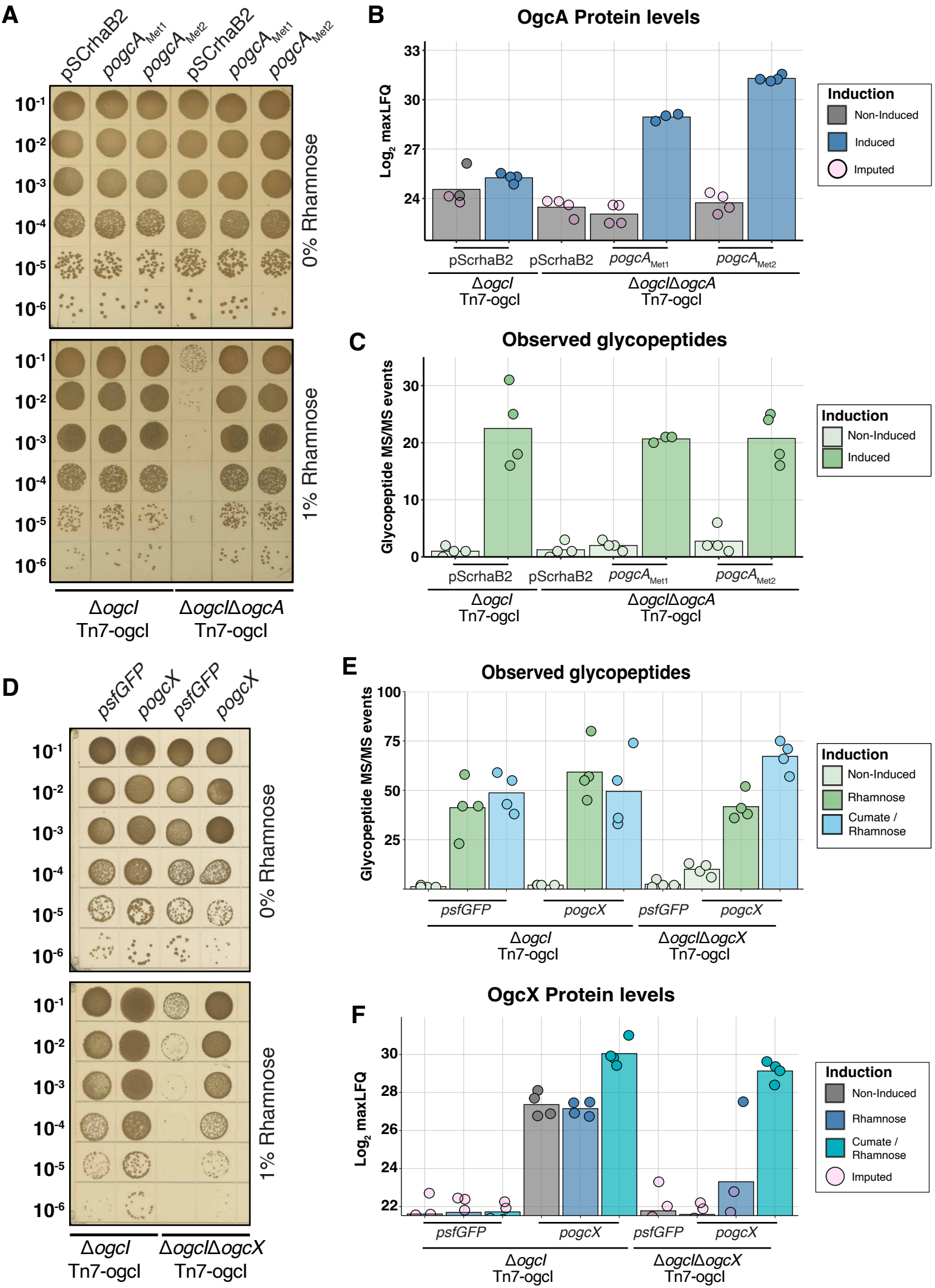
A
pSCrhaB2
pogcA Met1
pogcA Met2
pSCrhaB2
pogcA Met1
pogcA Met2
10-1
10-2
10-3
10-4
10-5
10-6
0% Rhamnose
1% Rhamnose
ΔogcI
Tn7-ogcI
ΔogcIΔogcA
Tn7-ogcI
B
OgcA Protein levels
Log2 maxLFQ
33
30
27
24
pScrhaB2
pScrhaB2
pogcA Met1
pogcA Met2
ΔogcI
Tn7-ogcI
ΔogcIΔogcA
Tn7-ogcI
Induction
Non-Induced
Induced
Imputed
C
Observed glycopeptides
Glycopeptide MS/MS events
30
20
10
0
pScrhaB2
pScrhaB2
pogcA Met1
pogcA Met2
ΔogcI
Tn7-ogcI
ΔogcIΔogcA
Tn7-ogcI
Induction
Non-Induced
Induced
D
psfGFP
pogcX
psfGFP
pogcX
10-1
10-2
10-3
10-4
10-5
10-6
0% Rhamnose
1% Rhamnose
ΔogcI
Tn7-ogcI
ΔogcIΔogcX
Tn7-ogcI
E
Observed glycopeptides
Glycopeptide MS/MS events
100
75
50
25
psfGFP
pogcX
psfGFP
pogcX
ΔogcI
Tn7-ogcI
ΔogcIΔogcX
Tn7-ogcI
Induction
Non-Induced
Rhamnose
Cumate / Rhamnose
F
OgcX Protein levels
Log2 maxLFQ
30
28
26
24
22
psfGFP
pogcX
psfGFP
pogcX
ΔogcI
Tn7-ogcI
ΔogcIΔogcX
Tn7-ogcI
Induction
Non-Induced
Rhamnose
Cumate / Rhamnose
Imputed

Figure 3

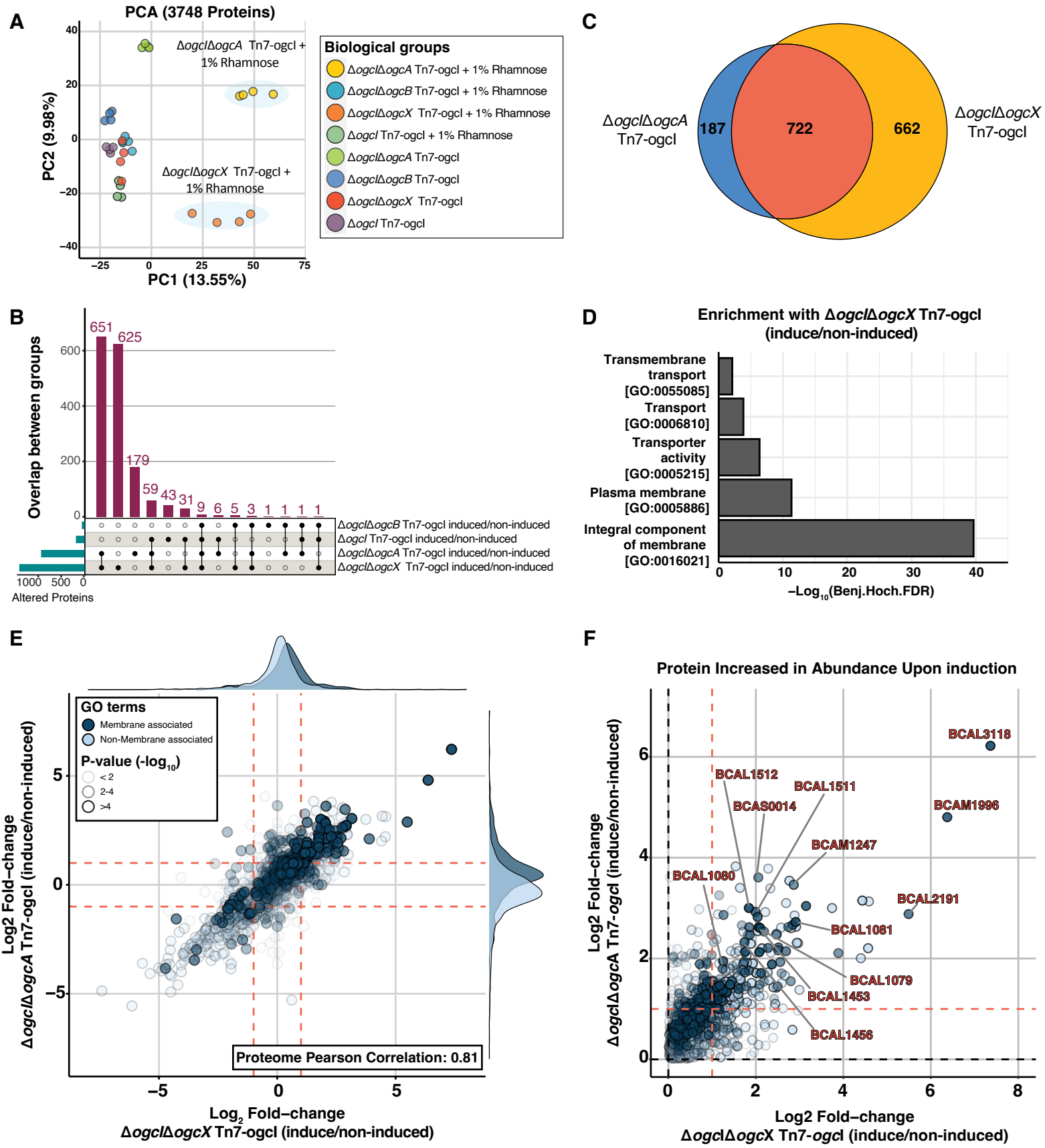
A
PCA (3748 Proteins)
ΔogclΔogcA Tn7-ogcl + 1% Rhamnose
ΔogclΔogcX Tn7-ogcl + 1% Rhamnose
PC2 (9.98%)
PC1 (13.55%)
Biological groups
ΔogclΔogcA Tn7-ogcl + 1% Rhamnose
ΔogclΔogcB Tn7-ogcl + 1% Rhamnose
ΔogclΔogcX Tn7-ogcl + 1% Rhamnose
Δogcl Tn7-ogcl + 1% Rhamnose
ΔogclΔogcA Tn7-ogcl
ΔogclΔogcB Tn7-ogcl
ΔogclΔogcX Tn7-ogcl
Δogcl Tn7-ogcl
C
ΔogclΔogcA Tn7-ogcl
187
722
662
ΔogclΔogcX Tn7-ogcl
B
Overlap between groups
651
625
179
59
43
31
9
6
5
3
1
1
1
1
ΔogclΔogcB Tn7-ogcl induced/non-induced
Δogcl Tn7-ogcl induced/non-induced
ΔogclΔogcA Tn7-ogcl induced/non-induced
ΔogclΔogcX Tn7-ogcl induced/non-induced
Altered Proteins
D
Enrichment with ΔogclΔogcX Tn7-ogcl (induce/non-induced)
Transmembrane transport [GO:0055085]
Transport [GO:0006810]
Transporter activity [GO:0005215]
Plasma membrane [GO:0005886]
Integral component of membrane [GO:0016021]
−Log10(Benj.Hoch.FDR)
E
GO terms
Membrane associated
Non-Membrane associated
P-value (-log10)
< 2
2-4
>4
Proteome Pearson Correlation: 0.81
Log2 Fold−change ΔogclΔogcA Tn7-ogcl (induce/non-induced)
Log2 Fold−change ΔogclΔogcX Tn7-ogcl (induce/non-induced)
F
Protein Increased in Abundance Upon induction
BCAL3118
BCAL1512
BCAL1511
BCAS0014
BCAM1996
BCAM1247
BCAL1080
BCAL2191
BCAL1081
BCAL1079
BCAL1453
BCAL1456
Log2 Fold−change ΔogclΔogcA Tn7-ogcl (induce/non-induced)
Log2 Fold−change ΔogclΔogcX Tn7-ogcl (induce/non-induced)

Figure 4

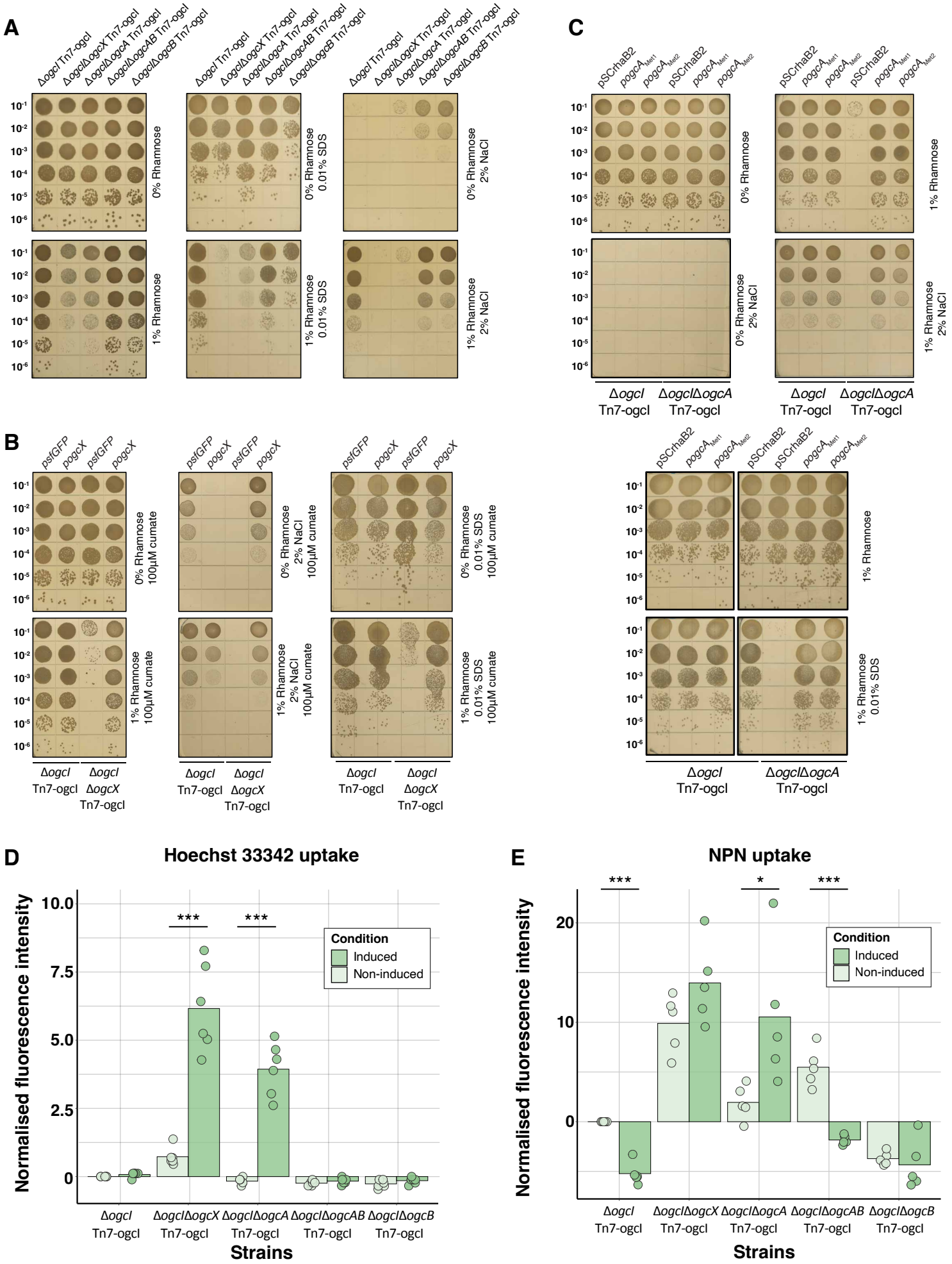
A
ΔogcI Tn7-ogcI
ΔogcIΔogcX Tn7-ogcI
ΔogcIΔogcA Tn7-ogcI
ΔogcIΔogcAB Tn7-ogcI
ΔogcIΔogcB Tn7-ogcI
0% Rhamnose
0% Rhamnose 0.01% SDS
0% Rhamnose 2% NaCl
1% Rhamnose
1% Rhamnose 0.01% SDS
1% Rhamnose 2% NaCl
B
psfGFP
pogcX
0% Rhamnose 100µM cumate
0% Rhamnose 2% NaCl 100µM cumate
0% Rhamnose 0.01% SDS 100µM cumate
1% Rhamnose 100µM cumate
1% Rhamnose 2% NaCl 100µM cumate
1% Rhamnose 0.01% SDS 100µM cumate
ΔogcI Tn7-ogcI
ΔogcI ΔogcX Tn7-ogcI
C
pSCrhaB2
pogcA Met1
pogcA Met2
0% Rhamnose
1% Rhamnose
0% Rhamnose 2% NaCl
1% Rhamnose 2% NaCl
1% Rhamnose 0.01% SDS
ΔogcI Tn7-ogcI
ΔogcIΔogcA Tn7-ogcI
D
Hoechst 33342 uptake
Normalised fluorescence intensity
Condition
Induced
Non-induced
***
ΔogcI Tn7-ogcI
ΔogcIΔogcX Tn7-ogcI
ΔogcIΔogcA Tn7-ogcI
ΔogcIΔogcAB Tn7-ogcI
ΔogcIΔogcB Tn7-ogcI
Strains
E
NPN uptake
*
Strains

Figure 5

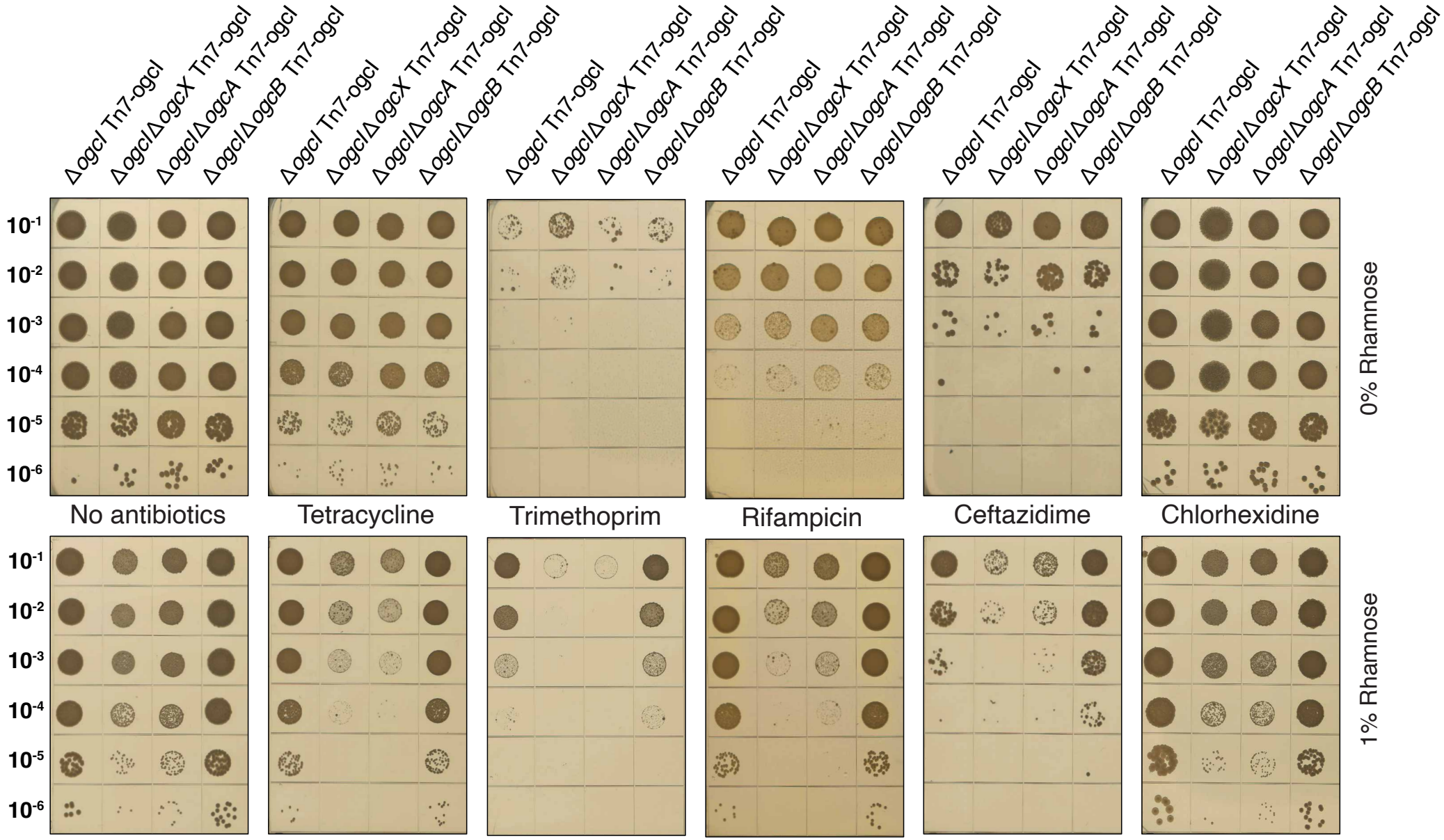
Δogcl Tn7-ogcl
ΔogclΔogcX Tn7-ogcl
ΔogclΔogcA Tn7-ogcl
ΔogclΔogcB Tn7-ogcl
10-1
10-2
10-3
10-4
10-5
10-6
No antibiotics
Tetracycline
Trimethoprim
Rifampicin
Ceftazidime
Chlorhexidine
0% Rhamnose
1% Rhamnose

Figure 6

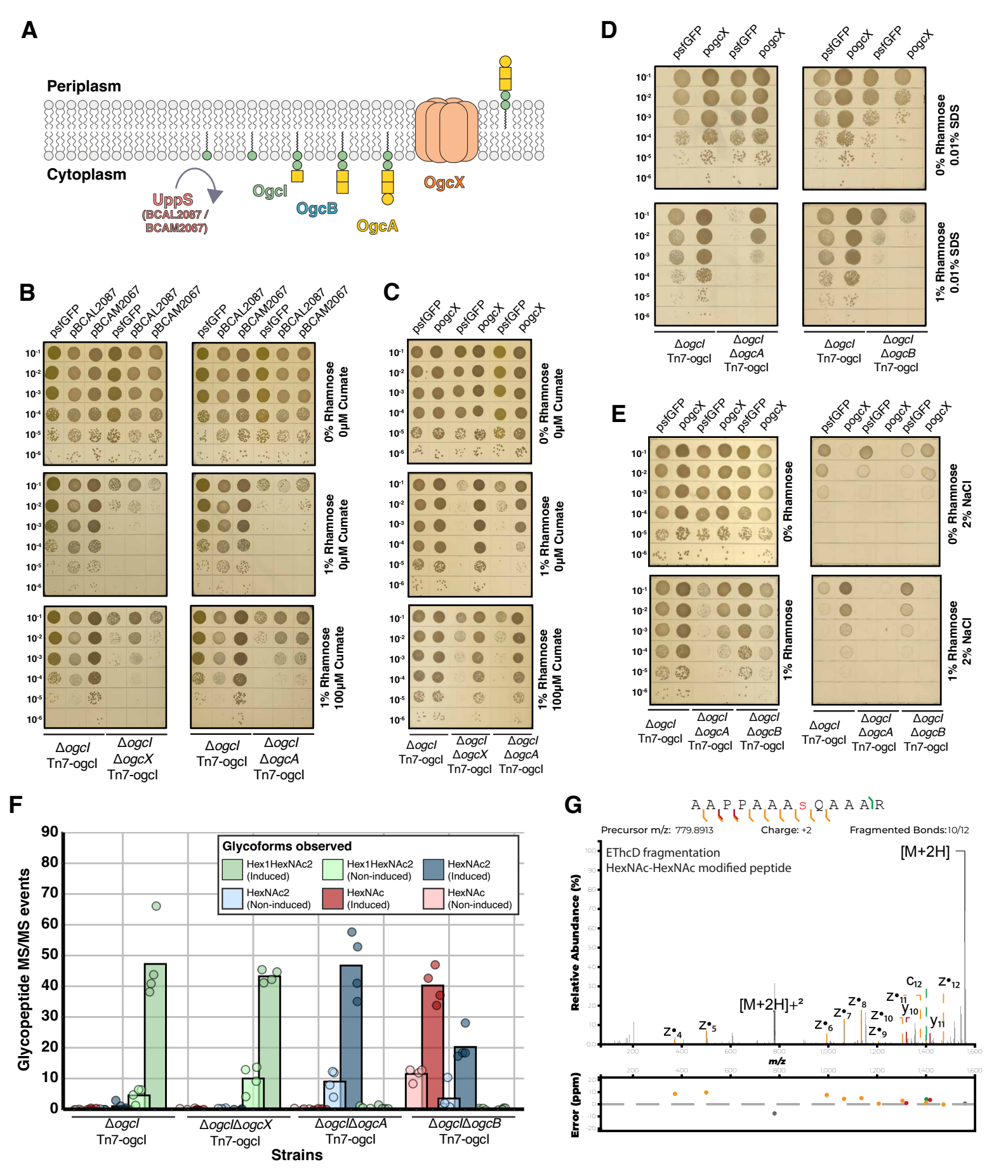
A
Periplasm
Cytoplasm
UppS
(BCAL2087 / BCAM2067)
OgcI
OgcB
OgcA
OgcX
B
psfGFP
pBCAL2087
pBCAM2067
0% Rhamnose 0μM Cumate
1% Rhamnose 0μM Cumate
1% Rhamnose 100μM Cumate
ΔogcI Tn7-ogcI
ΔogcI ΔogcX Tn7-ogcI
ΔogcI ΔogcA Tn7-ogcI
C
psfGFP
pogcX
D
0% Rhamnose 0.01% SDS
1% Rhamnose 0.01% SDS
ΔogcI Tn7-ogcI
ΔogcI ΔogcA Tn7-ogcI
ΔogcI ΔogcB Tn7-ogcI
E
0% Rhamnose
1% Rhamnose
0% Rhamnose 2% NaCl
1% Rhamnose 2% NaCl
F
Glycopeptide MS/MS events
Glycoforms observed
Hex1HexNAc2 (Induced)
Hex1HexNAc2 (Non-induced)
HexNAc2 (Induced)
HexNAc2 (Non-induced)
HexNAc (Induced)
HexNAc (Non-induced)
ΔogcI Tn7-ogcI
ΔogcIΔogcX Tn7-ogcI
ΔogcIΔogcA Tn7-ogcI
ΔogcIΔogcB Tn7-ogcI
Strains
G
AAPPAAAsQAAAR
Precursor m/z: 779.8913
Charge: +2
Fragmented Bonds: 10/12
EThcD fragmentation
HexNAc-HexNAc modified peptide
[M+2H]
[M+2H]+2
Relative Abundance (%)
m/z
Error (ppm)

Figure 7

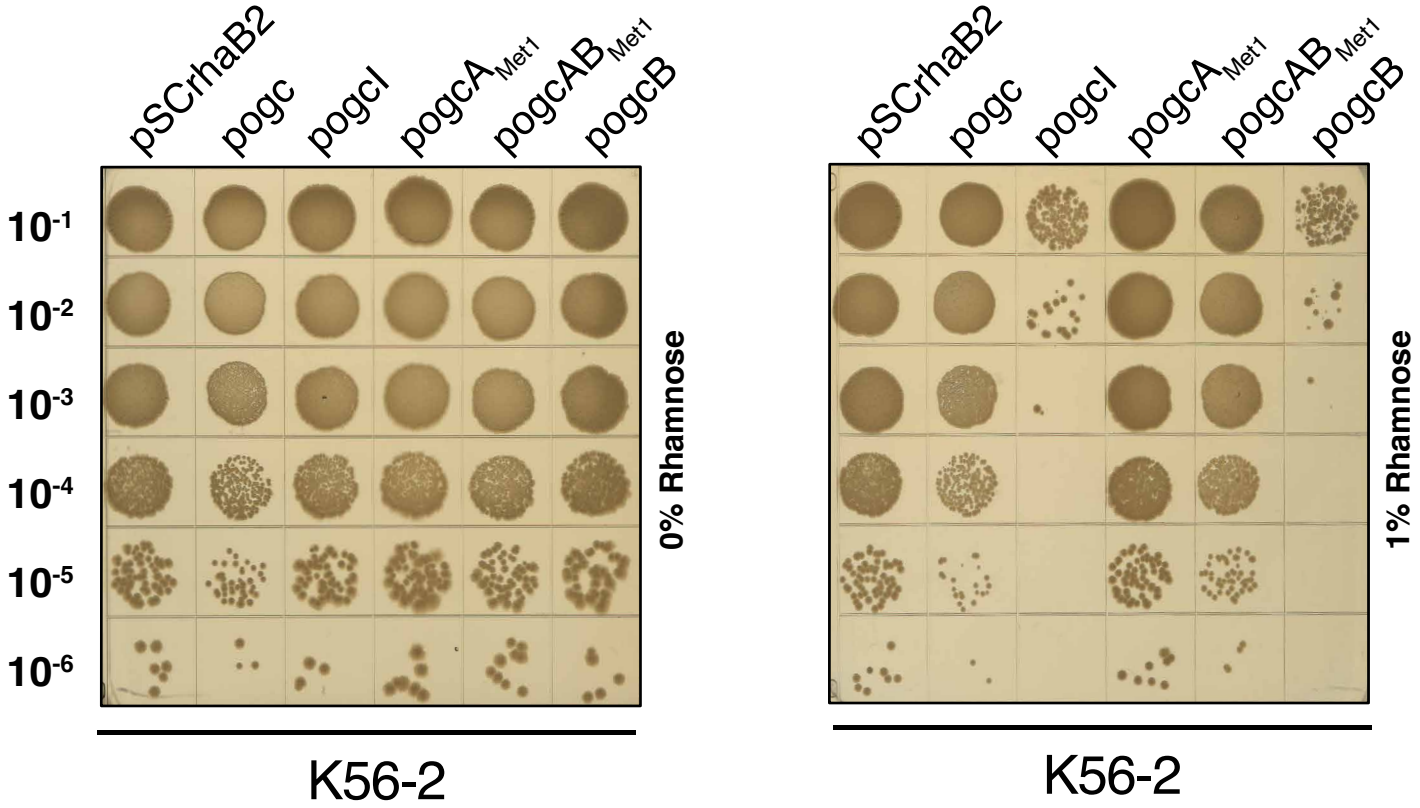
pSCrhaB2
pogc
pogcI
pogcA Met1
pogcAB Met1
pogcB
10-1
10-2
10-3
10-4
10-5
10-6
0% Rhamnose
K56-2
pSCrhaB2
pogc
pogcI
pogcA Met1
pogcAB Met1
pogcB
1% Rhamnose
K56-2

Figure 8